Research Square

Preprints are preliminary reports that have not undergone peer review.
They should not be considered conclusive, used to inform clinical practice,
or referenced by the media as validated information.

Clinical Efficacy of Multiparametric Magnetic Resonance Imaging and Proton Spectroscopy in the Evaluation of Complex Ring-Enhancing Intracranial Lesions: A Four-Case Series from Pacific International Hospital, Papua New Guinea

Messay Gebrekidan

mesayg@washington.edu

Pacific International Hospital https://orcid.org/0000-0001-6698-1321

Alfonso Blanch

Pacific International Hospital

Bina Basnet Thapa

Pacific International Hospital

Aamir Siddiqui

Pacific International Hospital https://orcid.org/0000-0003-2683-5340

Joel Nicolas

Pacific International Hospital

Jagan Abban

Pacific International Hospital

Tau Rawali

Pacific International Hospital

Case Report

Keywords: Ring-enhancing lesion, magnetic resonance spectroscopy, glioma, CNS tuberculoma, schwannoma, Papua New Guinea

Posted Date: September 29th, 2026

DOI: https://doi.org/10.21203/rs.3.rs-11168925/v1

License: This work is licensed under a Creative Commons Attribution 4.0 International License.
Read Full License

Additional Declarations: The authors declare no competing interests.

Clinical Efficacy of Multiparametric Magnetic Resonance Imaging and Proton Spectroscopy in the Evaluation of Complex Ring-Enhancing Intracranial Lesions: A Four-Case Series from Pacific International Hospital, Papua New Guinea

Experience from the Department of Radiology, Pacific International Hospital (PIH), Port Moresby, Papua New Guinea (June–September 2026)

Mesay Gebrekidan Woldecherkos[1,2], Alfonso Blanch[1], Bina Basnet Thapa[1], Aamir Siddiqui[1], Joel Nicolas[1], Jagan Abban[1], Tau Rawali[1]

1 Department of Radiology, Pacific International Hospital, 3 Mile, Port Moresby, Papua New Guinea

2 Tiru-Rad Diagnostics

Corresponding author: Mesay Gebrekidan Woldecherkos — Department of Radiology, Pacific International Hospital, Port Moresby, Papua New Guinea.

Highlights

- First Papua New Guinea case series correlating conventional MRI with single-voxel MR spectroscopy in ring-enhancing lesions.
- Elevated Cho/NAA and Cho/Cr ratios distinguished a cortical high-grade glioma from infective mimics.
- A lipid-lactate–dominant spectrum with low Cho/NAA supported caseating CNS tuberculoma.
- Overlapping tuberculoma and neurosarcoidosis phenotypes show the limits of spectroscopy alone.
- Strengthened referral pathways to advanced imaging centers can shorten time to diagnosis in PNG.

Abstract

Background: Ring-enhancing lesions (RELs) remain a persistent diagnostic challenge in neuroradiology, as neoplastic, infectious, and granulomatous processes frequently overlap in their conventional MRI appearance. Accurate differentiation is critical for guiding management, particularly in resource-limited settings such as Papua New Guinea (PNG), where access to advanced neuroimaging is concentrated in a few centers and specialist manpower is limited.

Study setting and design: This retrospective case series was conducted at Pacific International Hospital (PIH), Port Moresby, PNG, over four months (June–September 2026). Four brain MRI cases were included: three presenting as ring-enhancing masses, and one miscellaneous nerve sheath tumour at the craniocervical junction and C1–C2 level.

Materials and methods: Of the four cases, two were referred from Port Moresby General Hospital and two were managed in-house at PIH. Conventional MRI sequences, supplemented by single-voxel MR spectroscopy (MRS) in selected cases, were used to evaluate metabolite profiles and to help differentiate primary brain tumour, metastatic disease, and infective processes such as tuberculoma.

Results: One case, an 18-year-old male, demonstrated a cortical high-grade glioma with elevated choline-to-N-acetylaspartate (Cho/NAA >1.5) and choline-to-creatine (Cho/Cr >2) ratios, favouring a glial neoplasm despite an atypical age. A second case, a 29-year-old male with constitutional symptoms, showed multifocal ring-enhancing lesions with a preserved NAA peak and Cho/NAA <1, consistent with CNS tuberculoma and correlating with the clinical history. A third case demonstrated periventricular, splenial, and parieto-occipital rim-enhancing and serpentine lesions, radiologically indistinguishable between tuberculoma and neurosarcoidosis; tuberculoma was favoured on supporting clinical evidence. A fourth, miscellaneous case demonstrated a craniocervical/C1–C2 nerve sheath tumour with a characteristic dumbbell configuration on T2-FLAIR and post-contrast T1-weighted imaging.

Conclusion: This first PNG-based series demonstrates the added diagnostic value of MRS in characterising ring-enhancing lesions and illustrates how strengthened referral pathways from provincial and district-level facilities to centres equipped with advanced imaging can accelerate diagnosis and improve management outcomes.

Keywords: *Ring-enhancing lesion; magnetic resonance spectroscopy; glioma; CNS tuberculoma; schwannoma; Papua New Guinea*

1. Introduction

Magnetic resonance imaging (MRI) is a cornerstone of neuroimaging, providing unparalleled soft-tissue contrast for evaluating brain architecture and pathology. Among the many diagnostic dilemmas encountered in daily radiology practice, ring-enhancing lesions (RELs) are particularly demanding, as their morphology on conventional sequences is frequently shared across neoplastic, infectious, and inflammatory processes. In tuberculosis-endemic regions such as Papua New Guinea, this overlap is compounded by the high background prevalence of central nervous system (CNS) tuberculosis, which can closely mimic both primary and secondary brain tumors.

Magnetic resonance spectroscopy (MRS), when performed alongside conventional MRI, provides additional metabolic information that can be applied across a wide range of neurological conditions, including malignancy, cerebral ischemia, and traumatic brain injury [1]. MRS

evaluates the resonant frequencies and relative concentrations of key brain metabolites — including choline (Cho), creatine (Cr), and N-acetylaspartate (NAA) — which are represented as spectral peaks and amplitudes. Its findings are not diagnostic in isolation, however, and should always be interpreted alongside conventional MRI and the clinical context [2].

Advanced MRI techniques, and single-voxel MRS in particular, add a metabolic dimension to lesion characterization that is unavailable on conventional sequences alone. Elevated choline with reduced NAA reflects the increased membrane turnover and neuronal loss typical of neoplastic tissue, whereas a dominant lipid-lactate peak with a low choline-to-NAA ratio favours necrotic, caseating, or infective pathology such as tuberculoma [3]. To our knowledge, no prior case series from Papua New Guinea has directly characterized the imaging and spectroscopic patterns of ring-enhancing lesions. We present four unique cases evaluated at the PIH Radiology Department between June and September 2026, illustrating the combined value of conventional MRI and MRS and underscoring the broader theme of strengthening early referral pathways to advanced imaging within the provincial health system.

2. Materials and Methods

This is a retrospective, descriptive case series conducted at the Department of Radiology, Pacific International Hospital (PIH), Port Moresby, Papua New Guinea, over the four months from June to September 2026. Four brain MRI cases fulfilling the inclusion criteria were identified: three presented as ring-enhancing masses, and one was a miscellaneous nerve sheath tumor at the craniocervical junction and C1–C2 level, included for its educational value and unusual anatomic location.

Of the four cases, two were referred from Port Moresby General Hospital, where MRI was not functional at the time, and two were managed as in-house PIH patients. All patients underwent multiplanar, multisequence brain MRI, including T1- and T2-weighted imaging, T2-FLAIR, diffusion-weighted imaging (DWI) with apparent diffusion coefficient (ADC) mapping, susceptibility-weighted or gradient-echo imaging, and post-contrast T1-weighted sequences. Single-voxel MR spectroscopy (SVS) was performed in selected cases, with voxel placement over the most metabolically representative solid or enhancing component of each lesion. Key metabolite ratios, choline-to-NAA (Cho/NAA) and choline-to-creatine (Cho/Cr), were calculated and correlated with clinical presentation, available laboratory findings, and imaging morphology to reach the most likely diagnosis in each case.

3. Case Presentations

3.1 Case 1: High-grade cortical glioma in an 18-year-old male

Clinical presentation: An 18-year-old male presented with a six-month history of progressive left-sided upper- and lower-limb weakness, marked left upper-limb muscle atrophy, gait ataxia, headache, and intermittent numbness. He denied seizures, loss of consciousness, fever, or

constitutional symptoms. Examination confirmed left-sided motor weakness with upper-limb wasting.

MRI findings: A well-defined, intra-axial, cortically based lesion was centered within the right deep frontal lobe, with a thick, irregular peripheral wall that was predominantly hypointense on T1- and T2-weighted sequences, surrounding a centrally cystic/necrotic component (T1-hypointense, T2-hyperintense). No satellite lesions were seen. DWI showed restricted diffusion with low ADC values along the enhancing peripheral solid component, while the central cystic portion showed facilitated diffusion. No susceptibility artefact suggested calcification or hemorrhage. Despite the size of the lesion, surrounding vasogenic oedema and mass effect were minimal. Post-contrast imaging showed irregular, nodular peripheral enhancement with relative central non-enhancement.

MR spectroscopy: Single-voxel spectroscopy of the metabolically active peripheral solid component demonstrated a markedly elevated choline peak with reduced NAA, a Cho/NAA ratio >1.5, and a Cho/Cr ratio >2 — findings favoring an infiltrative glial neoplasm over infective granulomatous disease.

Imaging diagnosis: High-grade diffuse glioma, most likely anaplastic astrocytoma (WHO Grade 3) or an IDH-wild type diffuse astrocytic glioma with aggressive imaging features. Glioblastoma was considered less likely given the patient's age, the limited mass effect, and the relatively localized disease.

3.2 Case 2: CNS tuberculoma in a 29-year-old male

Clinical presentation: A 29-year-old male presented with left lower-limb weakness, unintentional weight loss, headache, and gait abnormality — a constellation raising concern for a chronic infective or granulomatous process.

MRI findings: A poorly defined ring-enhancing mass was identified at the right grey–white matter junction, with additional smaller ring-enhancing lesions in the left basal ganglia and cerebellum, indicating multifocal disease.

MR spectroscopy: SVS demonstrated a spectrum dominated by a lipid-lactate resonance with a preserved NAA peak and a Cho/NAA ratio <1 — a pattern characteristic of caseating CNS tuberculoma rather than neoplasm.

Imaging diagnosis: The multifocal distribution, the grey–white junction and deep grey/cerebellar involvement, and the lipid-lactate–predominant, low Cho/NAA spectroscopic pattern were consistent with CNS tuberculoma, correlating well with the patient's clinical history and systemic symptoms (weight loss, constitutional decline).

3.3 Case 3: Overlapping imaging pattern of CNS tuberculoma and neurosarcoidosis

Clinical presentation: A patient presented with new-onset seizures and left lower-limb weakness.

MRI findings: MRI demonstrated periventricular, splenial, and parieto-occipital rim-enhancing lesions together with serpentine-configured enhancing lesions — a pattern that can be seen in both granulomatous infection and CNS sarcoidosis. MRS showed a relative elevation of lipid resonance, favoring CNS tuberculosis over sarcoidosis, since neurosarcoidosis is a non-caseating granulomatous disease in which lipid resonances are typically unremarkable.

Imaging diagnosis: CNS tuberculoma and neurosarcoidosis were considered the leading differential diagnoses, as both entities can produce virtually identical periventricular and rim/serpentine enhancement patterns on conventional MRI. Clinical correlation, cerebrospinal fluid analysis, serum ACE level, chest imaging, and/or tissue diagnosis remain essential for definitive differentiation; tuberculoma was favored on the balance of supporting clinical evidence.

3.4 Case 4 (miscellaneous): Craniocervical/C1–C2 nerve sheath tumor

MRI findings: An incidentally diagnosed, well-defined extramedullary-extradural mass was identified at the craniocervical junction, extending to the C1–C2 level and demonstrating the characteristic 'dumbbell sign' as it extended through and expanded the neural exit foramen. This was seen on T2-FLAIR imaging as a bilobed, hyperintense lesion with a waist at the foraminal level, and confirmed on post-contrast T1-weighted imaging by avid, well-defined enhancement of both the intraspinal and extraspinal components. Chest radiography in this patient was unremarkable.

Imaging diagnosis: Findings were most consistent with a nerve sheath tumor (schwannoma) arising from a cervical nerve root, a benign, slow-growing peripheral nerve sheath tumor. Its inclusion in this series, although it is not a ring-enhancing lesion, reflects the diagnostic breadth encountered by a single radiology department in this setting and underscores the value of multiplanar MRI in defining lesion anatomy before surgical planning.

4. Discussion

This series brings together four cases that, despite differing pathology, share a common thread: each required advanced MRI beyond routine sequences to reach diagnostic clarity, and each arrived at PIH through a referral pathway that shaped how quickly that clarity was achieved.

MRS has demonstrated particular diagnostic and prognostic value in paediatric neuroimaging and may provide complementary metabolic information beyond structural MRI [4]. By assessing the presence and relative ratios of metabolites such as NAA, creatine, choline, and lactate, MRS can help characterise the nature and biological behaviour of abnormalities identified on conventional MRI [2]. Advances in faster MRS acquisition, with improved signal-to-noise ratio and spatial resolution, have further expanded its clinical utility by enabling detection of subtler metabolic alterations alongside the morphological and physiological changes seen in the surrounding brain parenchyma [5].

High-grade gliomas are uncommon in adolescents and young adults, and when cortically based and associated with minimal mass effect, as in Case 1, they can closely mimic an infective or granulomatous process [6] — a pitfall of particular relevance in a tuberculosis-endemic country such as Papua New Guinea. The distinction mattered clinically: an incorrect empirical diagnosis of tuberculoma in a young patient with an unrecognized glioma would have delayed tissue diagnosis and appropriate oncological management by months. MRS was decisive here [1,7]. Elevated choline, reflecting increased membrane turnover and cellular proliferation, together with reduced NAA (reflecting neuronal loss) and Cho/NAA and Cho/Cr ratios above 1.5 and 2, respectively, are patterns established in the literature as favoring neoplastic over infective tissue [1,8], and this held despite the patient's atypical age for a high-grade glioma.

Case 2 demonstrates the converse spectroscopic pattern. The multifocal ring-enhancing lesions at the grey–white junction, basal ganglia, and cerebellum, combined with a low Cho/NAA ratio, were characteristic of caseating CNS tuberculoma [3] a pattern well described in the neuroradiology literature, in which necrotic granulomas produce lipid and lactate resonances from anaerobic glycolysis and lipid-laden macrophages, rather than the elevated choline seen in viable, proliferating tumor tissue. The multifocality and grey–white junction predilection further supported a haematogenously disseminated infective process over a solitary primary neoplasm, and the patient's constitutional symptoms and weight loss reinforced this reading. The patient was referred to Internal Medicine and commenced on anti-tuberculous therapy (initial phase), with subsequent clinical improvement.

Case 3 illustrates a genuine limitation of imaging-based differentiation. Periventricular, splenial, and parieto-occipital rim-enhancing and serpentine lesions are a recognized shared phenotype of CNS tuberculoma and neurosarcoidosis [8,9], both of which preferentially involve the leptomeninges, perivascular (Virchow–Robin) spaces, and periventricular white matter. Unlike Case 2, spectroscopy alone could not reliably separate these entities in this case, reinforcing that MRS is a valuable adjunct rather than a stand-alone arbiter, and that ancillary work-up, cerebrospinal fluid analysis, serum ACE, chest CT for hilar lymphadenopathy, and ultimately tissue sampling remain necessary when the imaging phenotype is shared. Recent multicenter analyses combining conventional MRI with MRS continue to report improved diagnostic accuracy for lesion characterization when spectroscopy is added to standard sequences [10], which reinforces the value of the adjunctive metabolic assessment applied throughout the present series, even where, as in Case 3, it does not fully resolve the differential.

Case 4, while not a ring-enhancing lesion, is included for its educational and anatomical significance. The dumbbell configuration at the craniocervical junction and C1–C2 level, well demonstrated on T2-FLAIR and post-contrast T1-weighted imaging, is a classic sign of a nerve sheath tumour extending through an expanded neural foramen, and accurate pre-surgical delineation of the intraspinal and extraspinal components by MRI is essential for safe operative planning at this anatomically constrained level.

Taken together, these cases demonstrate that MRS meaningfully augments conventional MRI in the work-up of ring-enhancing lesions, but also that its diagnostic yield is pattern-dependent: highly informative when spectroscopic signatures diverge (Cases 1 and 2), and more limited when the underlying pathophysiology converges (Case 3). Equally important is the referral context in which these cases arose. Two of the four cases reached PIH only after initial evaluation at Port Moresby General Hospital, where advanced sequences such as MRS were not available locally. This series therefore supports the broader argument that strengthening early referral systems from provincial and district-level facilities to centers equipped with advanced neuroimaging capability directly shortens the diagnostic pathway, reduces reliance on empirical treatment, and enables more timely, targeted management — a theme of direct relevance to the ongoing review and strengthening of Provincial Health Authorities within Papua New Guinea's health system.

5. Learning Points

- Cortically based high-grade gliomas in young patients can closely mimic infective intracranial lesions, particularly in tuberculosis-endemic settings such as PNG.
- MR spectroscopy substantially improves diagnostic confidence: elevated choline with reduced NAA favours neoplasm, whereas a lipid-lactate–dominant spectrum with a low Cho/NAA ratio favours caseating tuberculoma, with the caveat of inherent limitations in interpreting lipid-lactate resonances on single-voxel MRS.
- CNS tuberculoma and neurosarcoidosis can be radiologically indistinguishable, particularly with periventricular, splenial, and serpentine rim-enhancing patterns; clinical, laboratory, and histopathological correlation remains essential in such cases, and correlation with chest radiography or other peripheral systems is also worthwhile.
- The dumbbell sign on T2-FLAIR and post-contrast T1-weighted imaging reliably indicates a nerve sheath tumour extending through an expanded neural foramen and is critical for pre-surgical planning; most such tumours, including schwannoma, show minimal or no contrast enhancement beyond the expected pattern.
- Strengthening early referral pathways from provincial hospitals to centres with advanced neuroimaging capability, including MRS, can meaningfully shorten time to diagnosis and improve management outcomes in resource-limited settings, alongside parallel gains in neurosurgical service quality.

6. Limitations

This study is limited by its use of single-voxel MRS, which requires manual placement of the voxel over the most active focus of a ring-enhancing lesion along a single axis, unlike multivoxel MRS, which allows spatial mapping of metabolite distribution across the entire lesion. In addition, histopathological confirmation of the glioma case was delayed following neurosurgical sampling. PIH has already confirmed plans to upgrade its MRI system to a multivoxel- and MR-perfusion–

capable scanner within the next few months, which will enable more comprehensive advanced neuroimaging at this PNG facility and support improved neurological case detection and neurosurgical service delivery.

7. Conclusion

This Papua New Guinea–based case series demonstrates the complementary diagnostic value of conventional MRI and single-voxel MR spectroscopy in characterising ring-enhancing brain lesions, spanning primary neoplasm, infective granulomatous disease, and lesions with overlapping neoplastic–infective imaging phenotypes, alongside an anatomically instructive nerve sheath tumour. Beyond the commonly assumed tuberculoma burden at PIH Radiology, this series also identified a notable proportion of primary malignant tumours confirmed by MRS. Accurate differentiation between malignant and granulomatous (tuberculoma) lesions in resource-limited settings such as PNG is essential for optimising neurosurgical planning, improving surgical outcomes, and enhancing overall diagnostic service delivery.

Acknowledgments

We would like to acknowledge the PIH Radiology Department imaging staff for their support in compiling the imaging data and facilitating MRS acquisition for selected cases. We also sincerely thank the PIH clinical and administrative leadership for their support and cooperation throughout this case series.

CRediT Authorship Contribution Statement

Mesay Gebrekidan Woldecherkos: Conceptualization, Methodology, Image and spectroscopy analysis, writing – original draft, writing – review & editing, Supervision. Alfonso Blanch, Bina Basnet Thapa and Aamir Siddiqui: Data curation, writing – review & editing. Joel Nicolas, Jagan Abban and Tau Rawali: Image acquisition and data preparation. All authors read and approved the final manuscript.

Declarations

Ethical considerations: Written informed consent was obtained from the patients for inclusion of all four cases in this case series. Patient confidentiality and anonymity were strictly maintained throughout the preparation and presentation of the cases, with no personally identifiable information disclosed.

Funding: No funding was allocated for this research.

Conflict of interest: The authors disclose no conflict of interest.

Data availability: The imaging datasets analysed during the current case series are available from

the corresponding author and the PIH PACS repository on reasonable request.

References

[1] Seth, R., Kalra, V., Sharma, U. and Jagannathan, N. (2010) 'Magnetic resonance spectroscopy in ring enhancing lesions', Indian Pediatrics, 47(9), pp. 803–804.

[2] Bulakbasi, N. (2004) 'Clinical applications of proton MR spectroscopy in the diagnosis of brain tumours', Trends in Neurovascular Imaging, pp. 143–153.

[3] Mukherjee, S., Das, R. and Begum, S. (2015) 'Tuberculoma of the brain — a diagnostic dilemma: magnetic resonance spectroscopy a new ray of hope', The Journal of Association of Chest Physicians, 3(1), p. 3.

[4] Lequin, M. and Hendrikse, J. (2017) 'Advanced MR imaging in pediatric brain tumors, clinical applications', Neuroimaging Clinics of North America, 27(1), pp. 167–190.

[5] Vallée, R., Vallée, J.N., Guillevin, C., Lallouette, A., Thomas, C., Rittano, G., Wager, M., Guillevin, R. and Vallée, A. (2023) 'Machine learning decision tree models for multiclass classification of common malignant brain tumors using perfusion and spectroscopy MRI data', Frontiers in Oncology, 13, 1089998.

[6] Iqbal, S., Khan, M.U.G., Saba, T. and Rehman, A. (2017) 'Computer-assisted brain tumor type discrimination using magnetic resonance imaging features', Biomedical Engineering Letters, 8(1), pp. 5–28.

[7] Riley, C.S., Roth, L.A., Sampson, J.B., Radhakrishnan, J., Herlitz, L.C., Blitz, A.M. and Moazami, G. (2017) 'A 31-year-old man with a ring-enhancing brain lesion', Journal of Neuro-Ophthalmology, 37(2), pp. 172–175.

[8] Shetty, G., Avabratha, K.S. and Rai, B.S. (2014) 'Ring-enhancing lesions in the brain: a diagnostic dilemma', Iranian Journal of Child Neurology, 8(3), pp. 61–64.

[9] Bhiraju, S.S., John, E., Raza, R.A., Ahmed, M., Fengas, L. and Hussain, S.H.Z. (2025) 'The radiological mimicry of ring-enhancing lesions: cerebral toxoplasmosis masquerading as metastatic disease', Cureus, 17(9), e92604.

[10] Anandavel, T.T., Yuvabalakumaran, G., Pravitha, B., Sathiyanarayanan, R. and Sachin, S.B. (2025) 'Role of MRI in evaluation of ring enhancing lesion in brain in correlation with MR spectroscopy', Bulletin of Stomatology and Maxillofacial Surgery, 21(8), pp. 144–153.

Figures

Case no. 1: Right frontal convexity mass demonstrating irregular ring enhancement with a central necrotic segment.

- **Figure 1A:** Structural T1-weighted sagittal view
- **Figure 1B:** Structural T1-weighted axial acquisition
- **Figure 1C-1D:** DWI assessment with corresponding ADC mapping
- **Figure 1D:** T1-weighted post-gadolinium MR imaging
- **Figure 1E:** SVS demonstrating metabolic signatures (Cho/NAA and Cho/Cr >1.5)

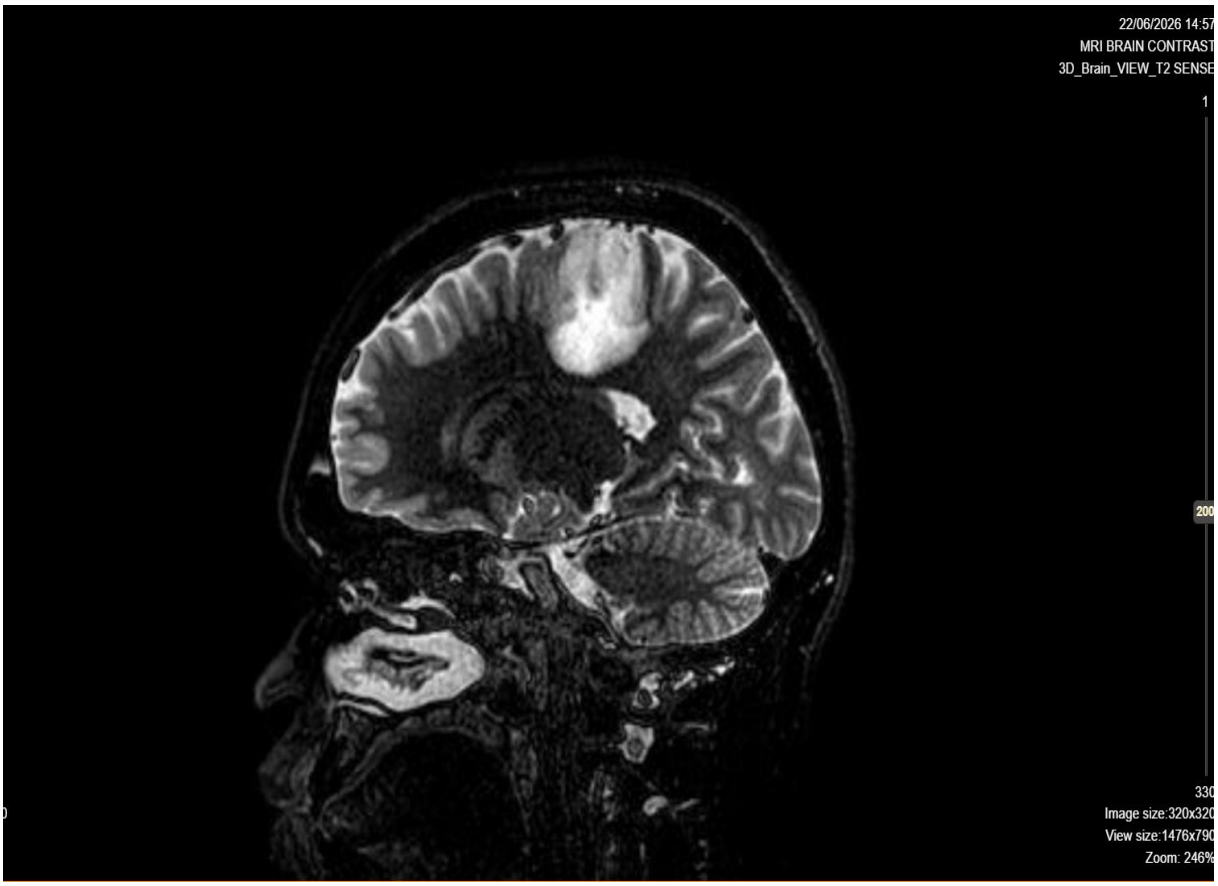

Figure 1A. Mid-sagittal T2-weighted sequence acquisition.

Figure 1B. Axial and coronal T1-weighted sequences demonstrate an intra-axial, cortical-based mass within the deep right frontal lobe. The peripheral wall exhibits hypointense to isointense T1

signal surrounding a central necrotic/cystic core that mimics CSF. There is negligible mass effect, and no susceptibility features suggestive of calcification.

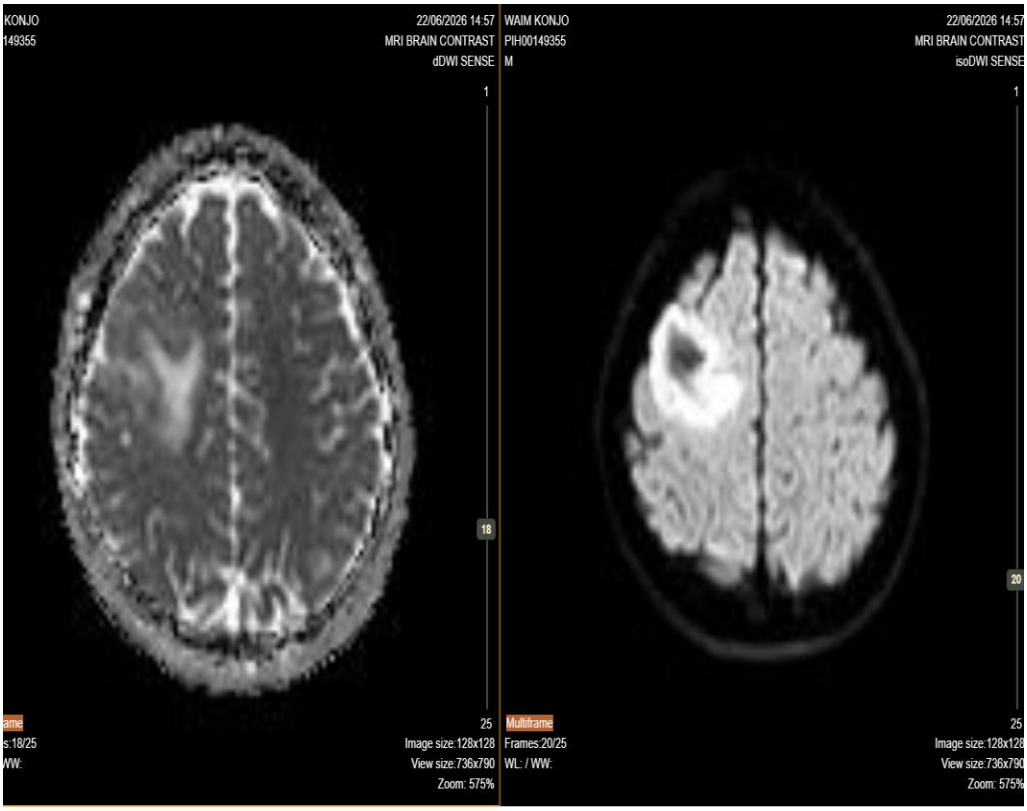

Figure 1C–D. Diffusion-weighted imaging (DWI) paired with apparent diffusion coefficient (ADC) maps demonstrate restricted diffusion along the peripheral wall, consistent with high cellularity, while the internal cystic component shows facilitated diffusion.

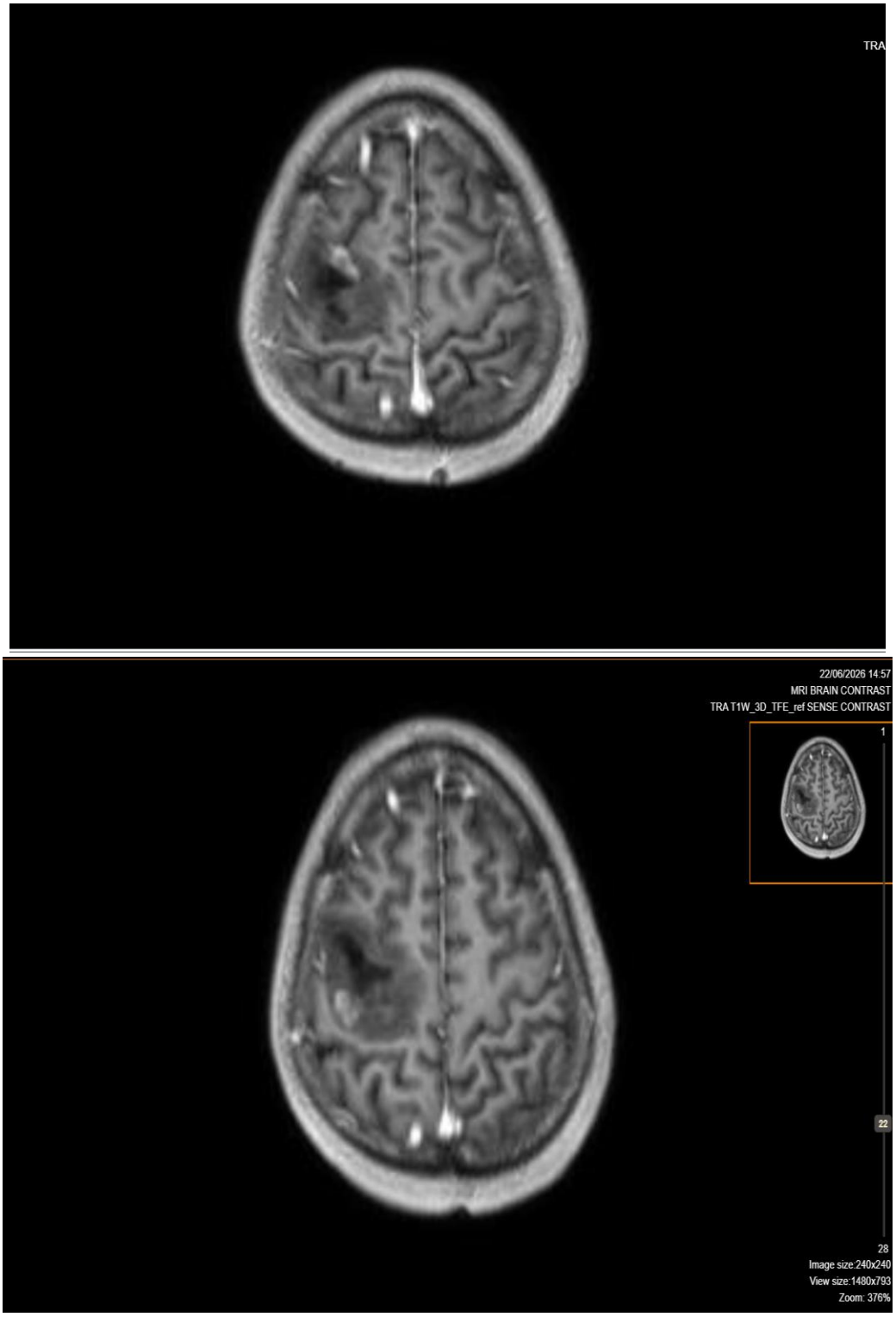

Figure 1D. Post-contrast T1-weighted imaging highlights irregular, nodular peripheral enhancement of the thickened wall. The central region demonstrates a lack of enhancement, consistent with internal liquefactive tumor necrosis.

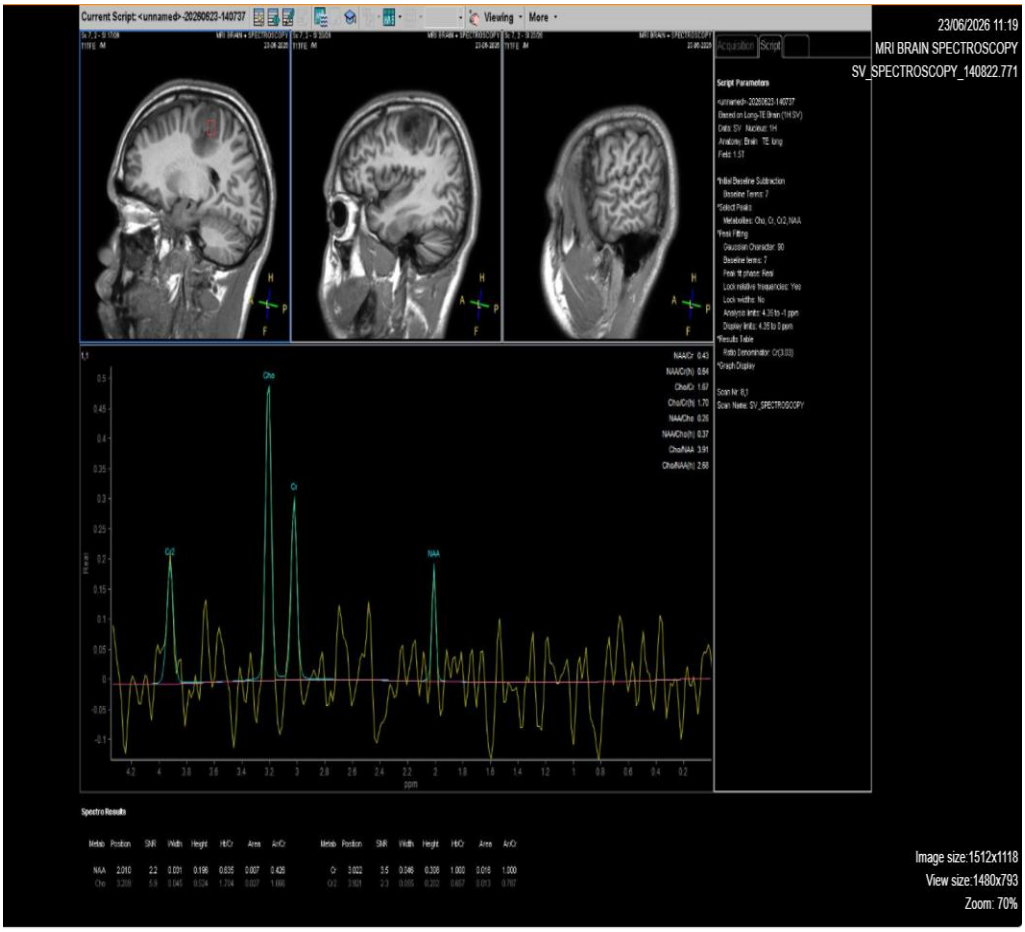

- **Figure 1E.** Single-voxel MR spectroscopy (SVS) targeted at the metabolically representative peripheral component reveals a dominant choline peak with Cho/NAA and Cho/Cr ratios >1.5. This profile, combined with neuronal loss (reduced NAA), strongly favors an infiltrative glial neoplasm.

Case 2: Multifocal Ring-Enhancing Lesions Correlating with Multiple CNS Tuberculomas Confirmed with raised NAA(NAA/Cho ratio >1)

A 49-year-old male presented with a clinical constellation including headache, gait abnormality, constitutional weight loss, and left-sided motor weakness.

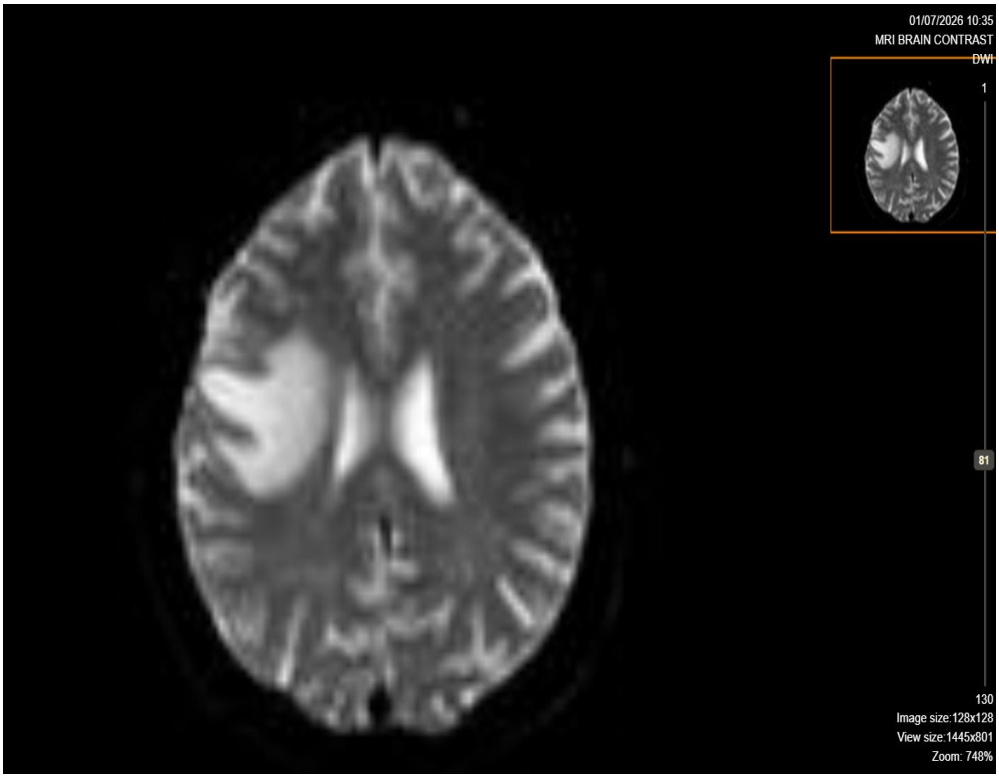
01/07/2026 10:35
MRI BRAIN CONTRAST
DWI
1
81
130
Image size:128x128
View size:1445x801
Zoom: 748%

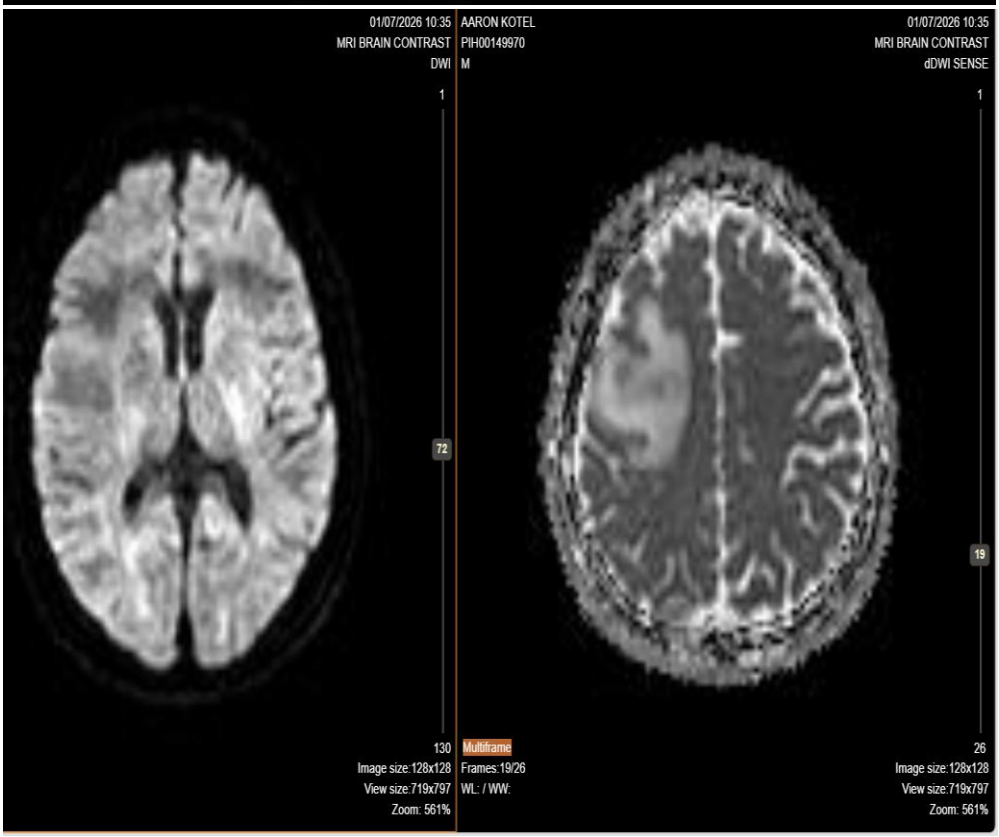
01/07/2026 10:35
MRI BRAIN CONTRAST
DWI
1
72
130
Image size:128x128
View size:719x797
Zoom: 561%
AARON KOTEL
PIH00149970
M
Multiframe
Frames:19/26
WL: / WW:
01/07/2026 10:35
MRI BRAIN CONTRAST
dDWI SENSE
1
19
26
Image size:128x128
View size:719x797
Zoom: 561%

Figure 2A: Diffusion-weighted imaging and ADC mapping analysis.

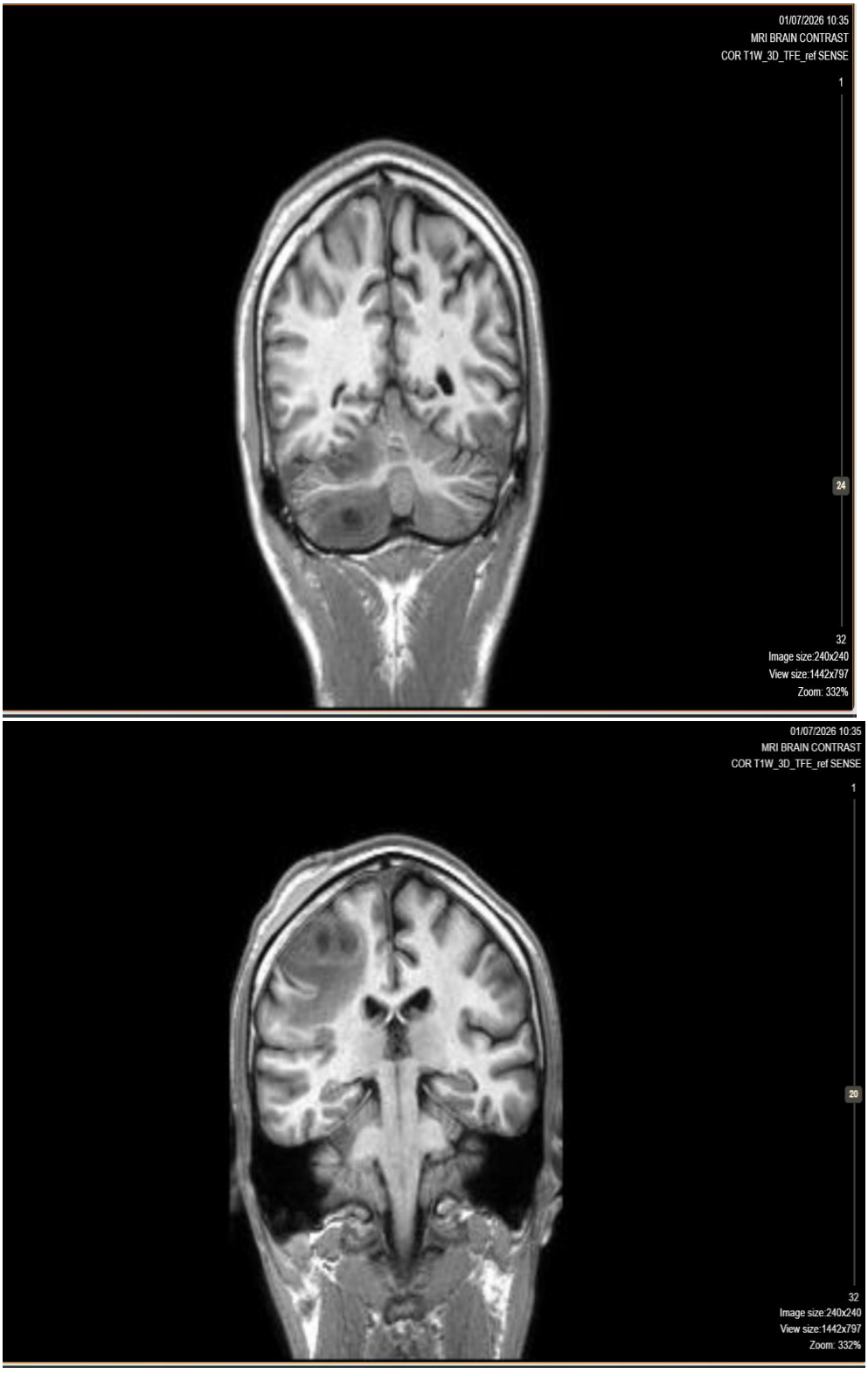

Figure 2B. Coronal T2-FLAIR imaging demonstrating right-sided frontal and deep gray matter involvement.

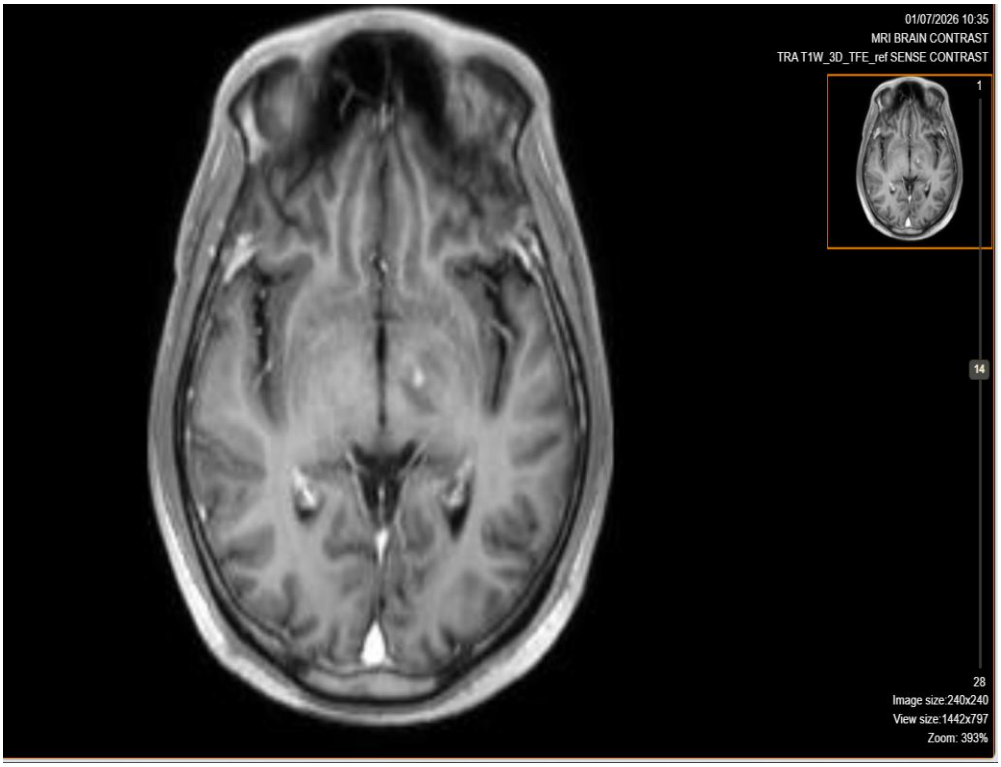

Figure 2C. Representative ring-enhancing mass identified within the left basal ganglia.

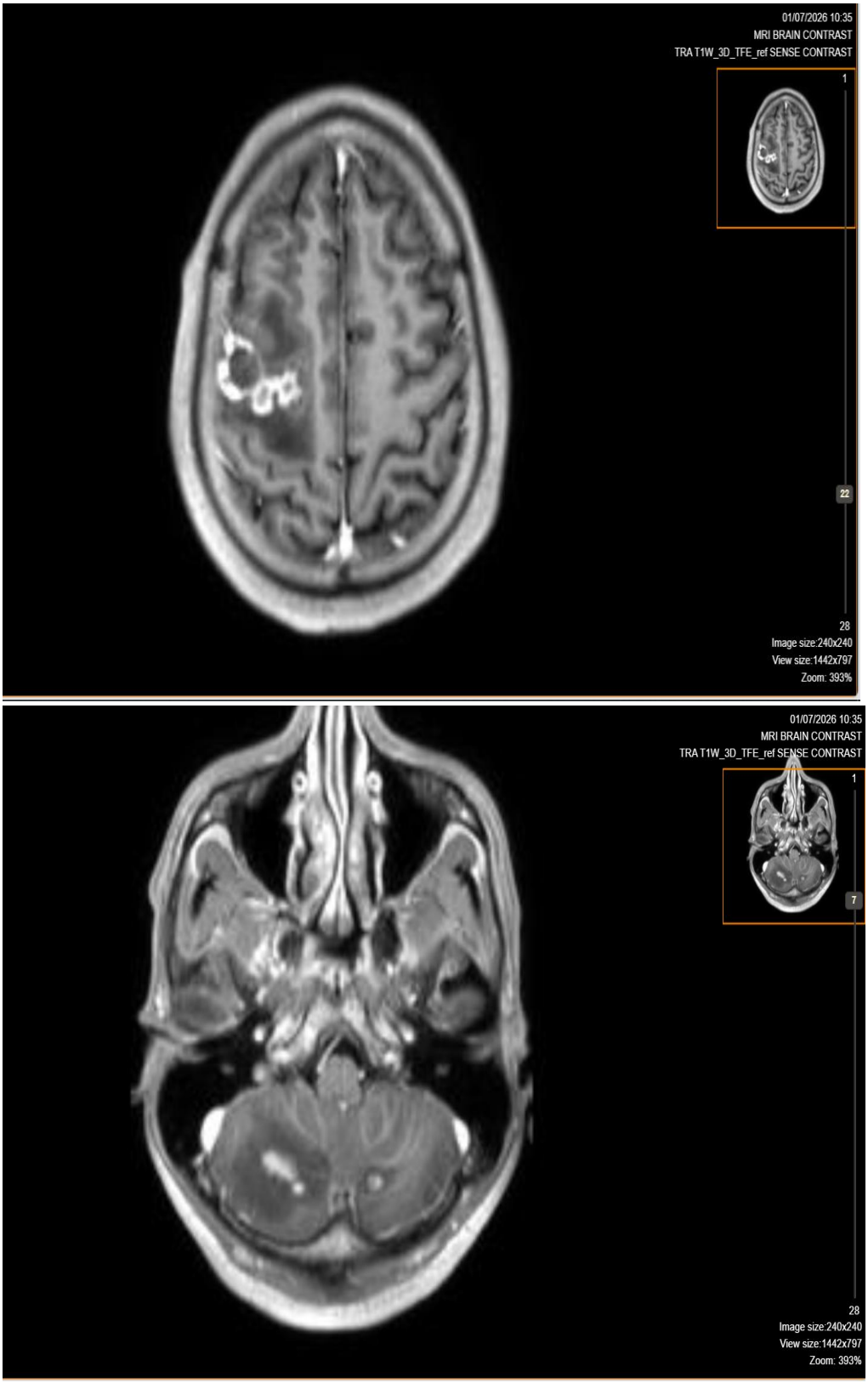

Figure 2D. Right-sided cortical and infratentorial cerebellar ring-enhancing lesions.

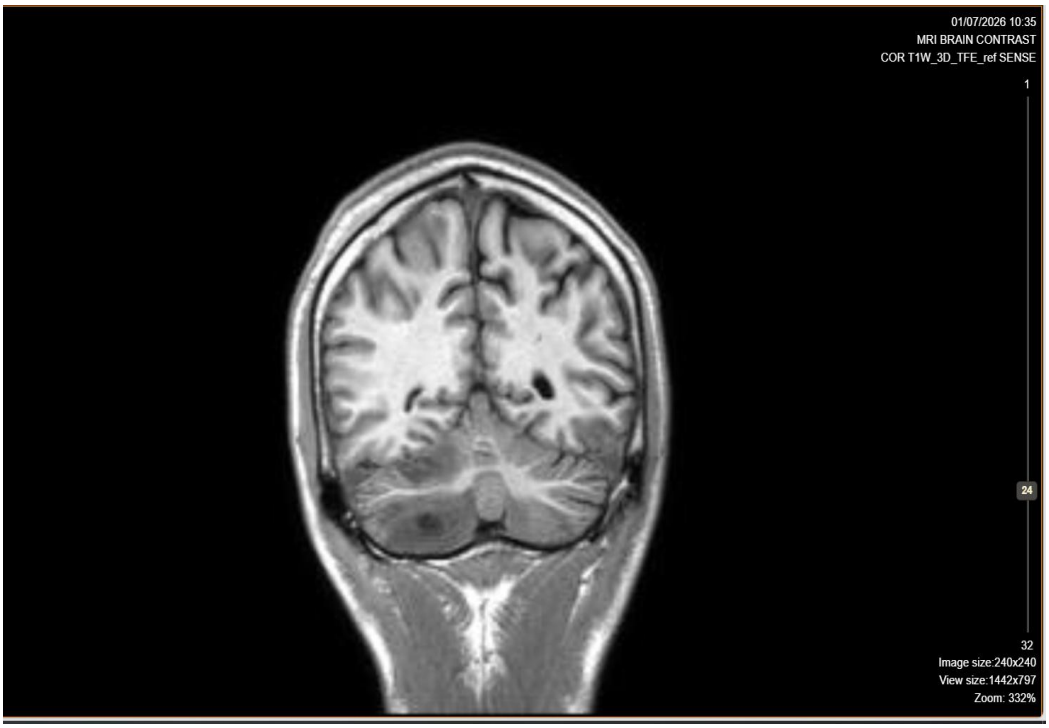

Figure 2E. Coronal T2-FLAIR sequence acquisition.

Figure 2F: Sagittal T2-FLAIR reveals a hyperintense mass with a characteristic hypointense internal mural nodule.

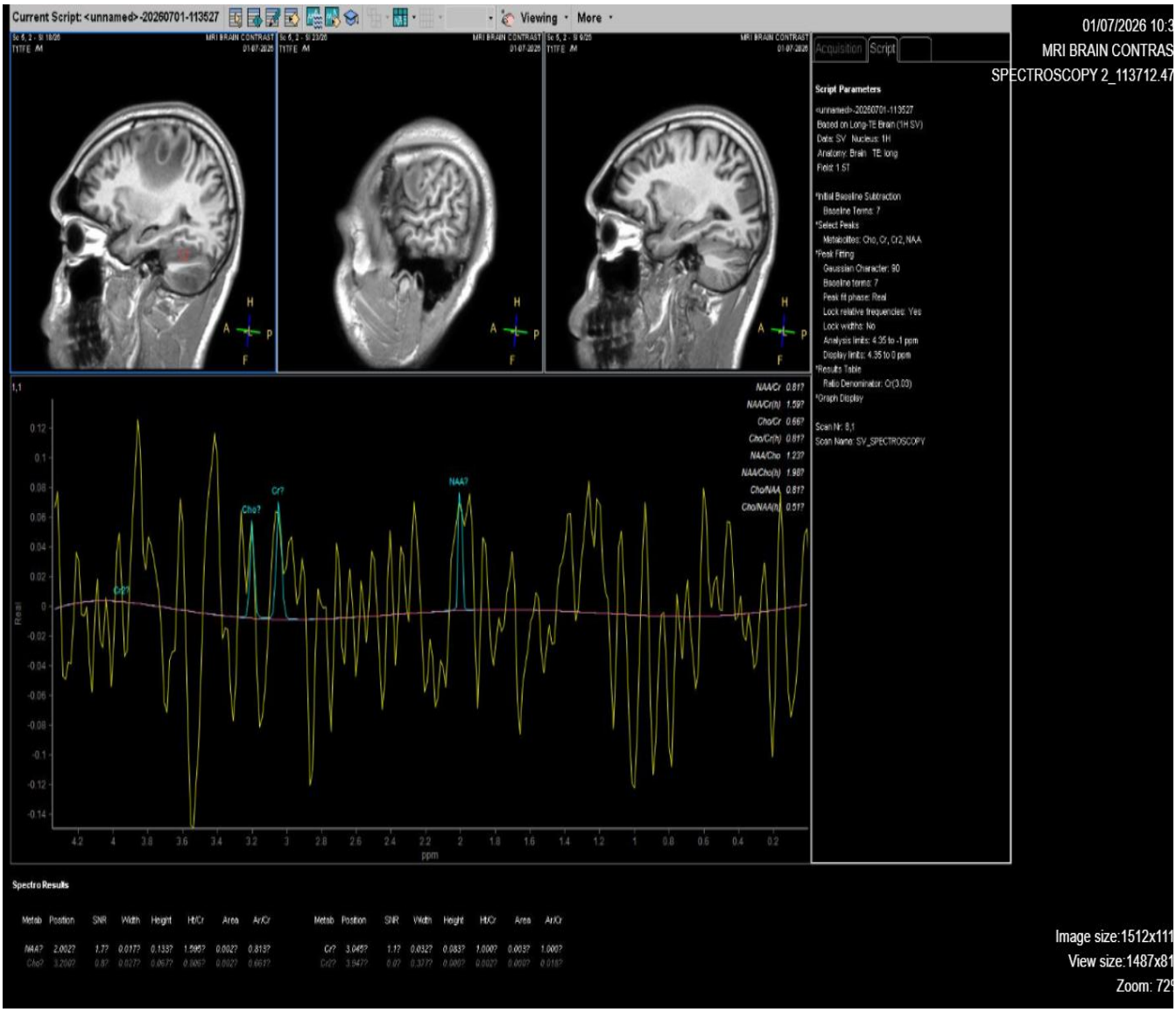

Figure 2G: There is increased NAA/Cho and NAA/Cr ratios (>1) on selected active ROIs from the lesions, suggestive of a granulomatous TB infectious process rather than a malignant tumor.

Case 3: Complex Multiloculated Ring-Enhancing Lesions Favoring CNS Tuberculoma

A 54-year-old female with known cardiovascular disease presented with progressive headache and left motor deficits. Imaging demonstrates multiloculated lesions involving the splenium, parieto-occipital white matter, and periventricular regions, with an incidental arachnoid cyst.

01/07/2026 12:42
MRI BRAIN PLAIN
SAG_Brain_VIEW_T2 SENSE
1
24
50
Image size:320x320
View size:1612x877
Zoom: 274%

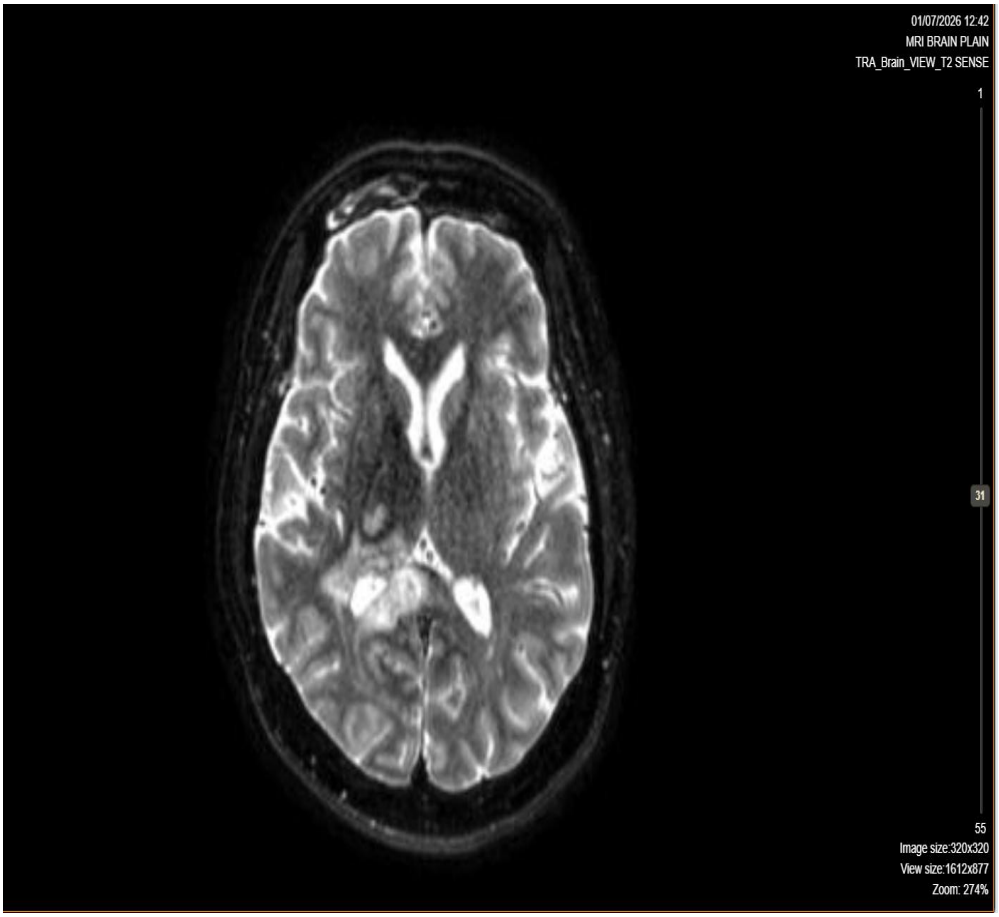

Figure 3A: Sagittal and axial structural T2-weighted acquisitions.

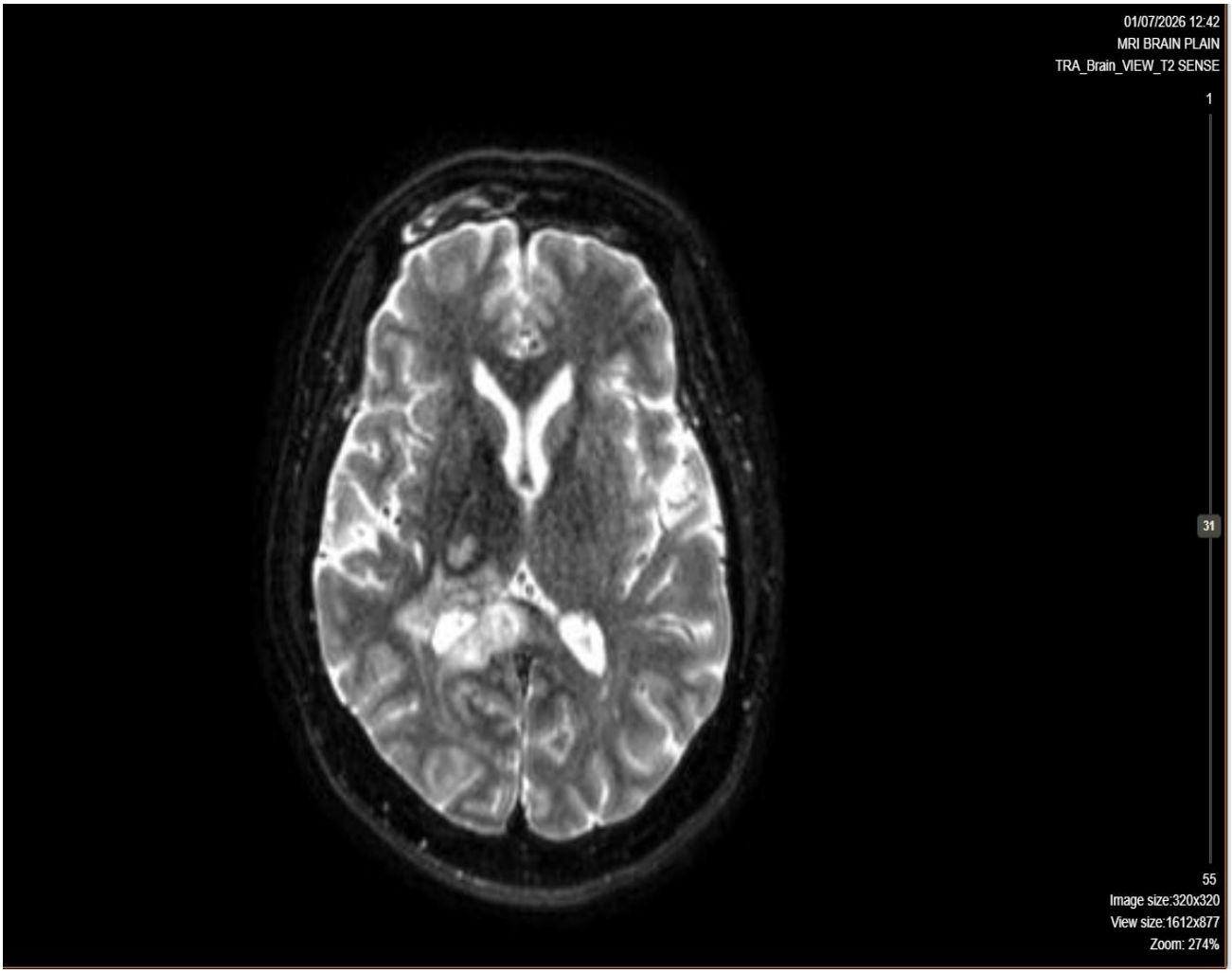
01/07/2026 12:42
MRI BRAIN PLAIN
TRA_Brain_VIEW_T2 SENSE
1
31
55
Image size:320x320
View size:1612x877
Zoom: 274%

Figure 3B: Axial T2 Fast Spin Echo (FSE) imaging.

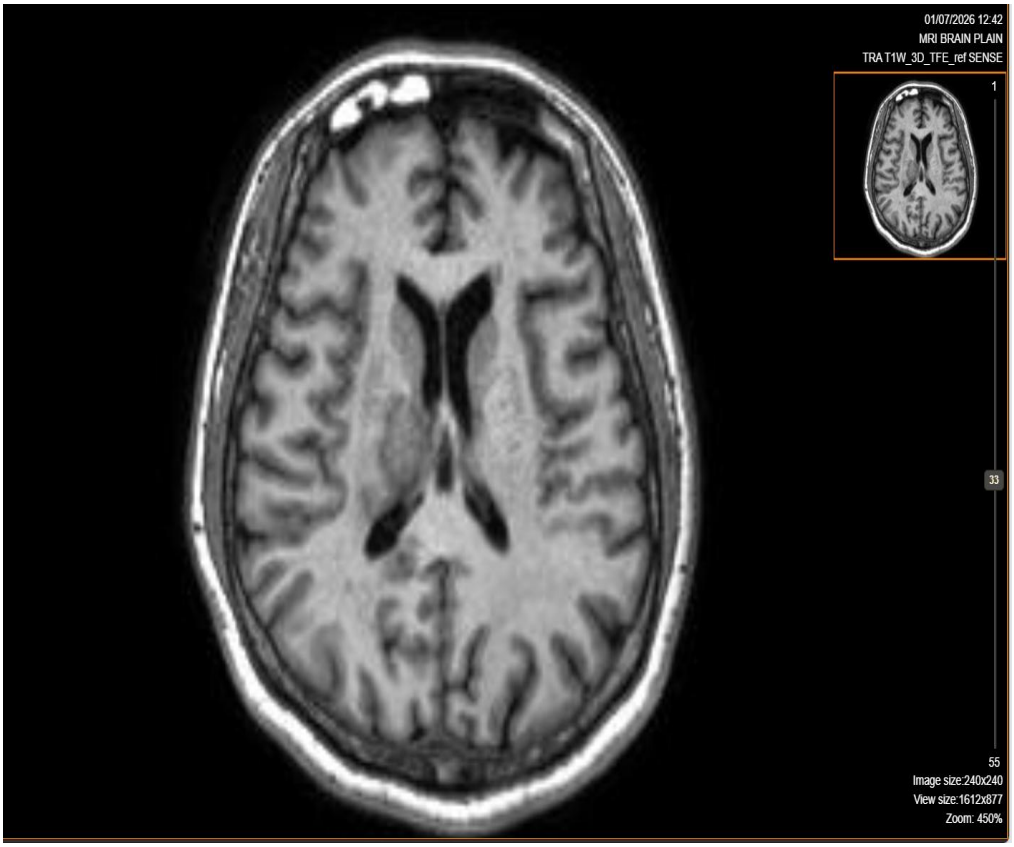
01/07/2026 12:42
MRI BRAIN PLAIN
TRA T1W_3D_TFE_ref SENSE
1
33
55
Image size:240x240
View size:1612x877
Zoom: 450%

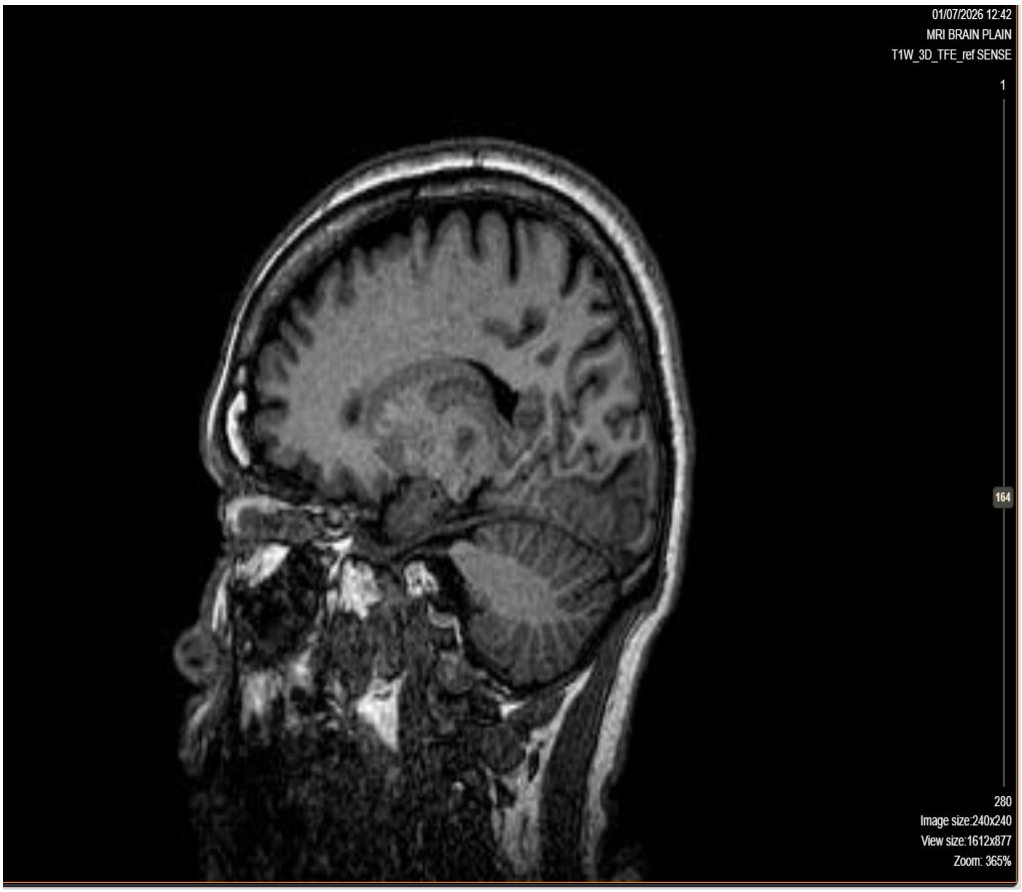
01/07/2026 12:42
MRI BRAIN PLAIN
T1W_3D_TFE_ref SENSE
1
164
280
Image size:240x240
View size:1612x877
Zoom: 365%

Figure 3C. Axial and sagittal T1-weighted structural imaging.

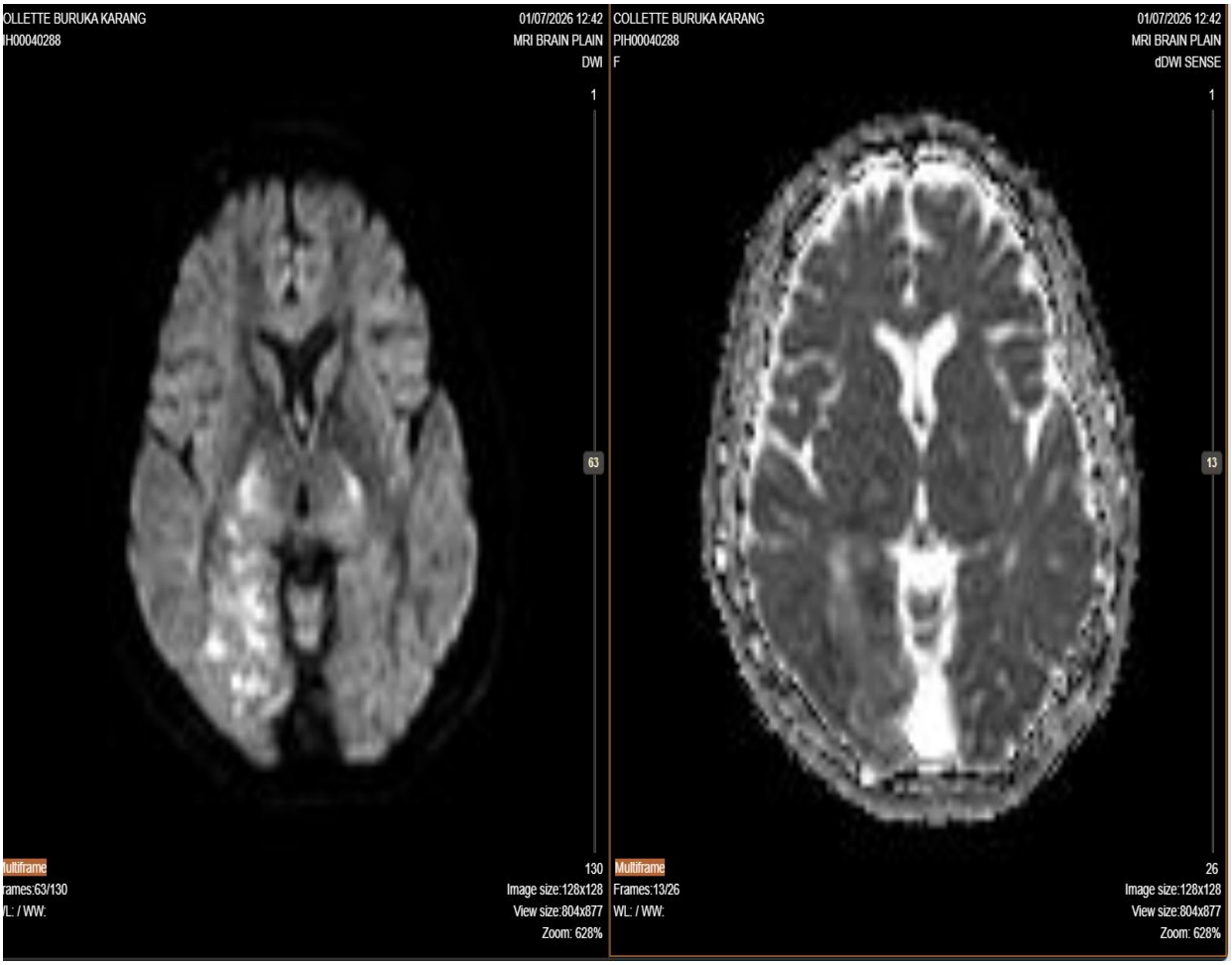

Figure 3D: Diffusion-weighted imaging and ADC mapping analysis showing gyral diffusion restriction.

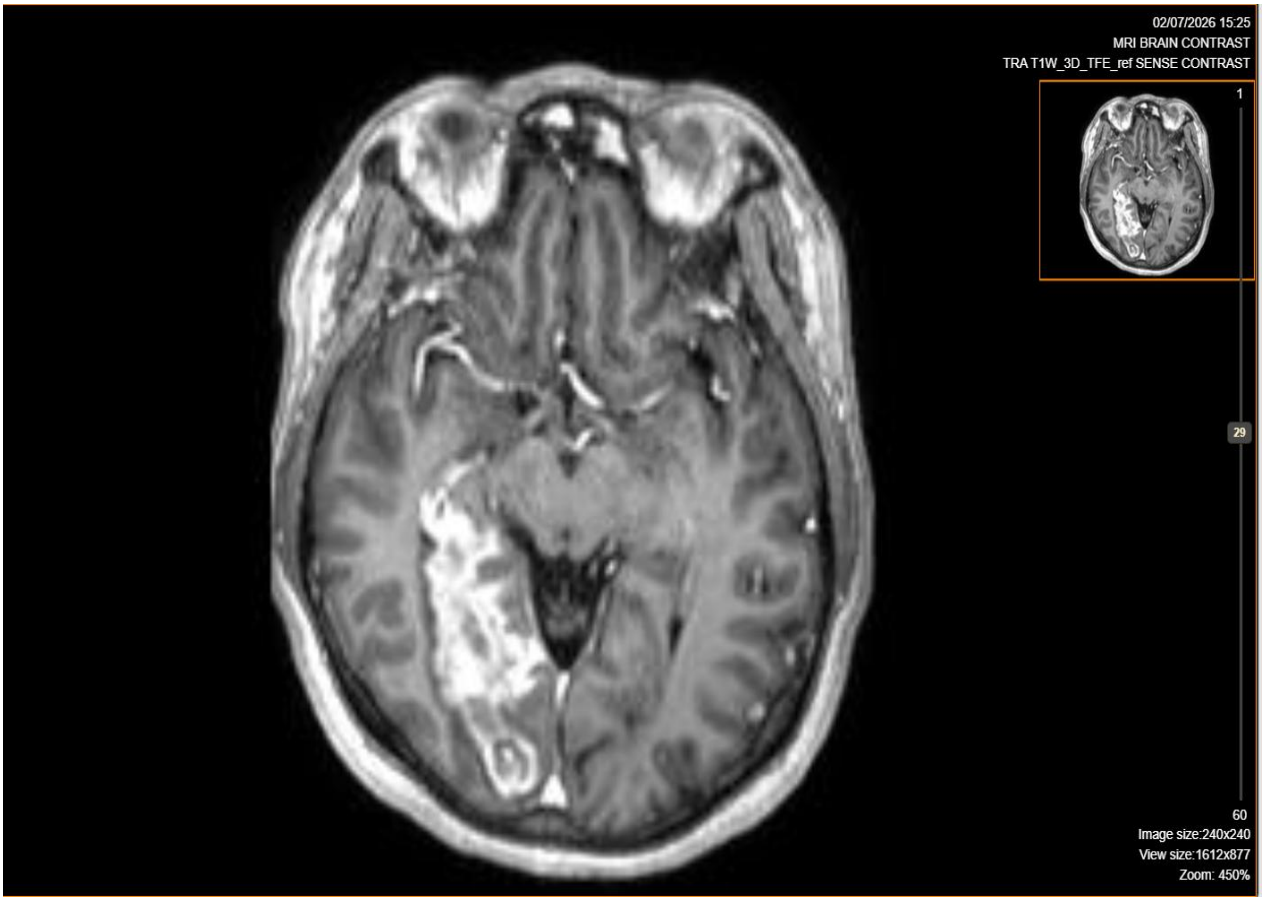
02/07/2026 15:25
MRI BRAIN CONTRAST
TRA T1W_3D_TFE_ref SENSE CONTRAST
1
29
60
Image size:240x240
View size:1612x877
Zoom: 450%

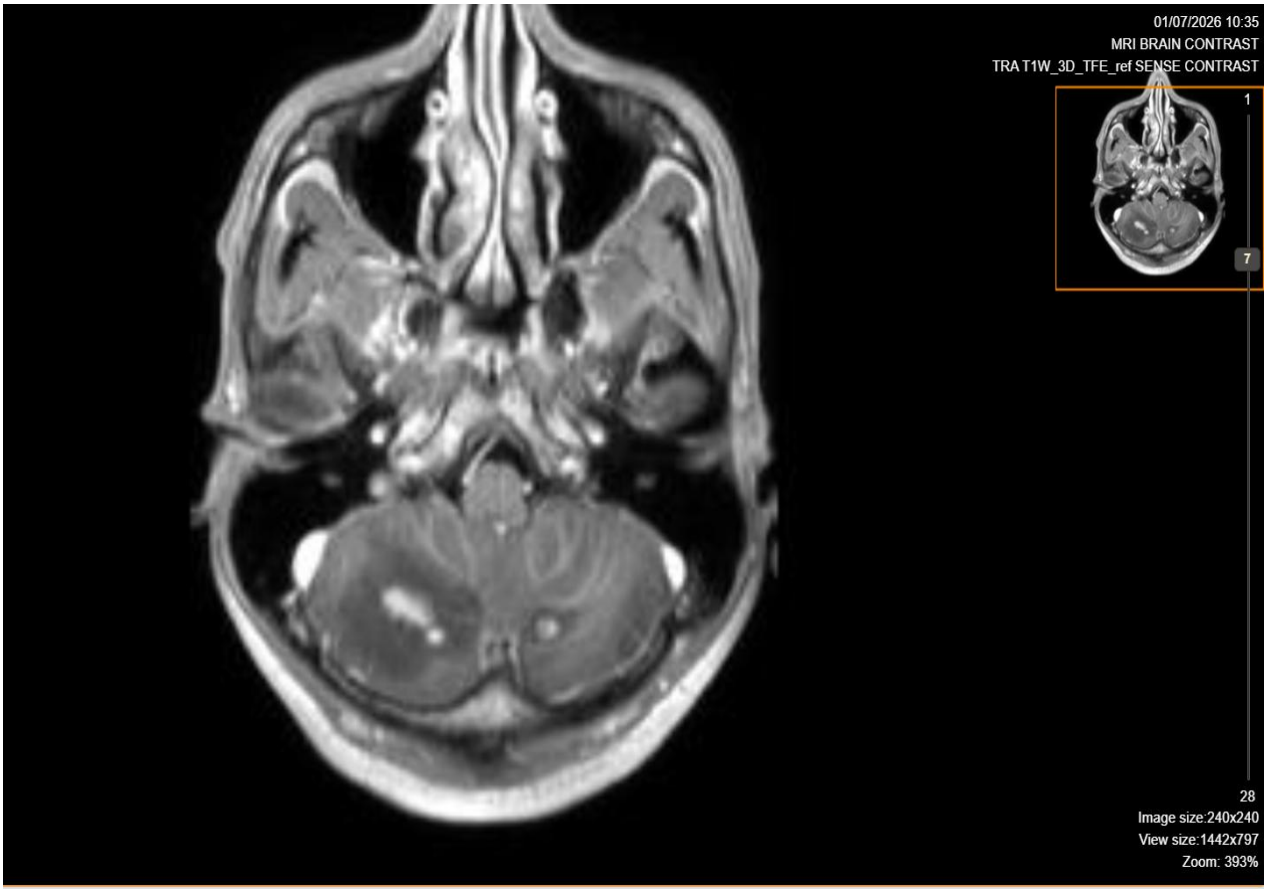
01/07/2026 10:35
MRI BRAIN CONTRAST
TRA T1W_3D_TFE_ref SENSE CONTRAST
1
7
28
Image size:240x240
View size:1442x797
Zoom: 393%

Figure 3E: Post-gadolinium axial T1-weighted images demonstrate ring- and nodular-enhancing lesions.

Figure 3F: Post-gadolinium sagittal T1-weighted distribution: periventricular and para-tentorial lesions.

01/07/2026 12:42
MRI BRAIN PLAIN
TRA_Brain_VIEW_FLAIR SENSE
1
35
50
Image size:256x256
View size:1612x877
Zoom: 342%

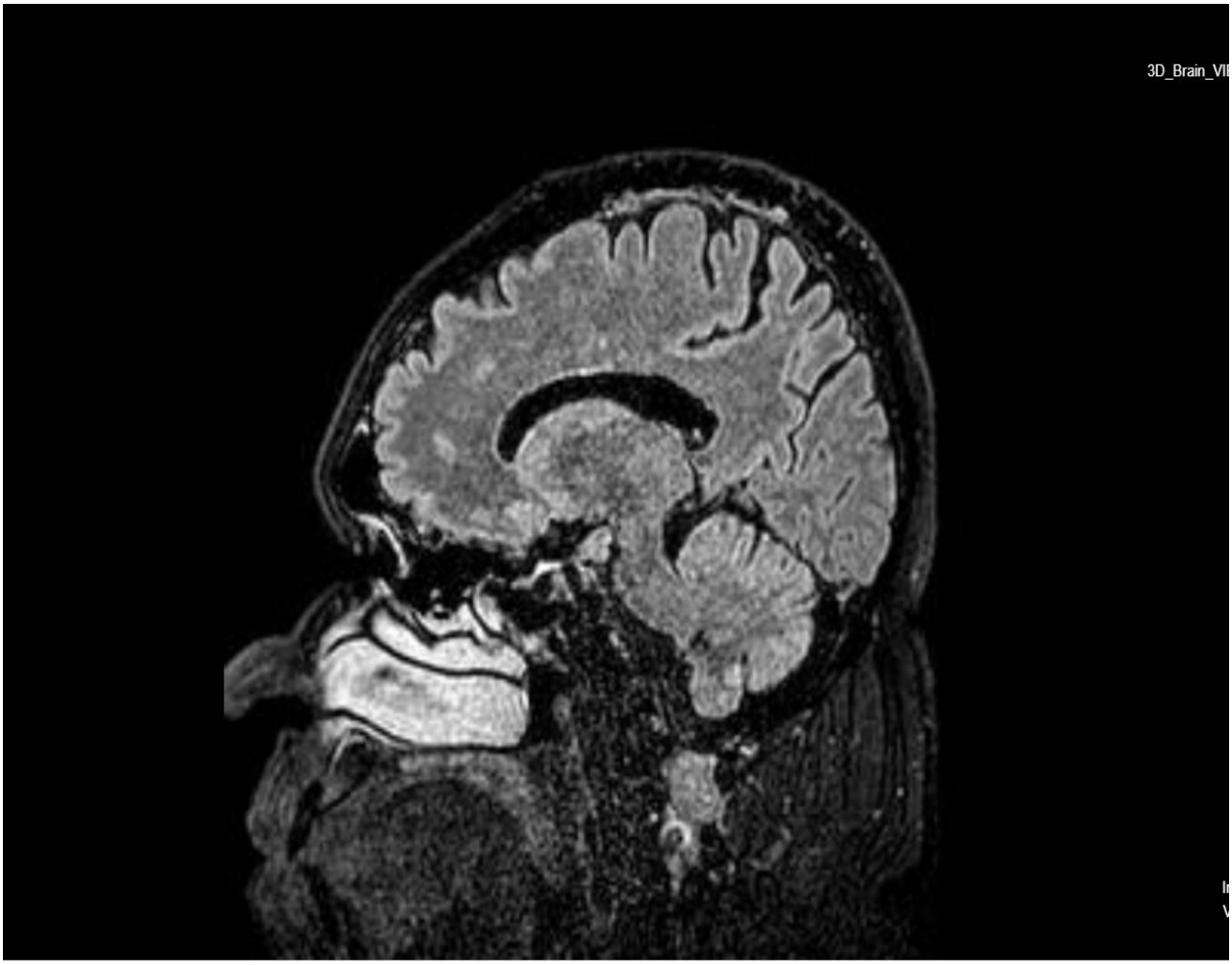
3D_Brain_VI

Figure 3G: Axial and sagittal T2-FLAIR sequence series.

Clinical context remains consistent with the aforementioned 54-year-old female patient presenting with acute neurological deficits.

01/07/2026 12:42
MRI BRAIN PLAIN
SAG_Brain_VIEW_T2 SENSE
1
24
50
Image size:320x320
View size:1612x877
Zoom: 274%

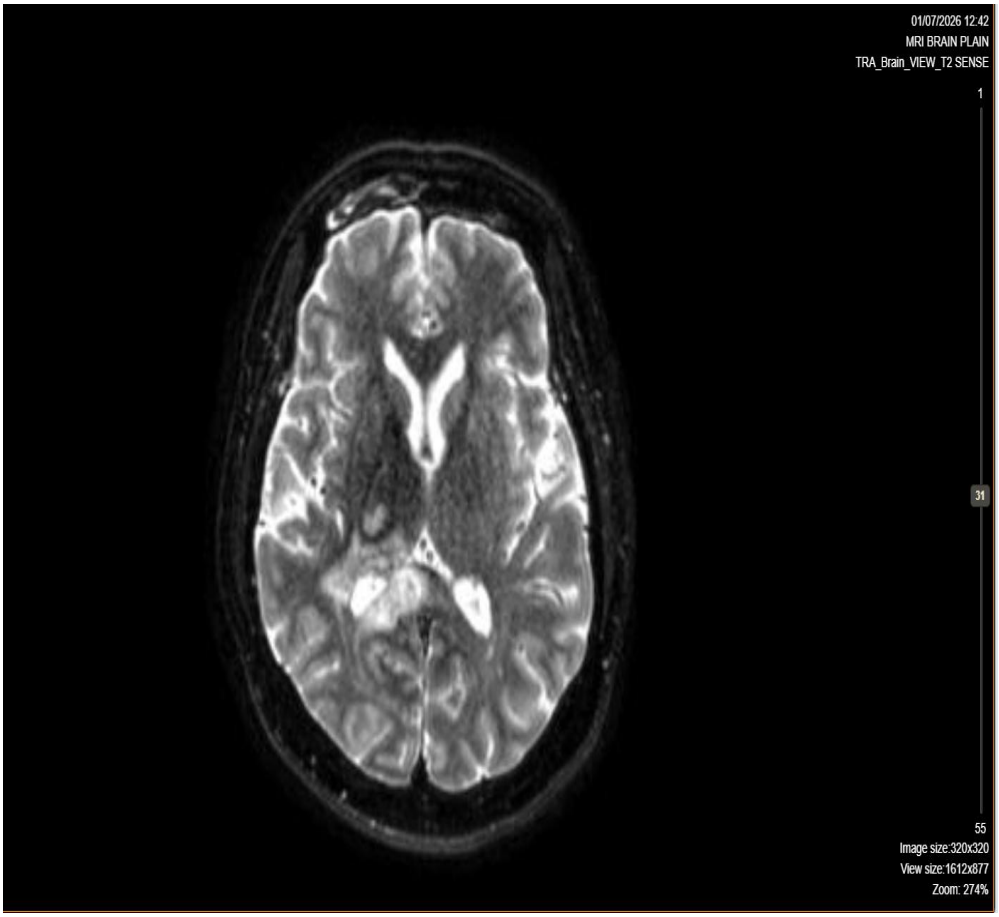

Figure 3H. Multiplanar T2-weighted structural acquisitions.

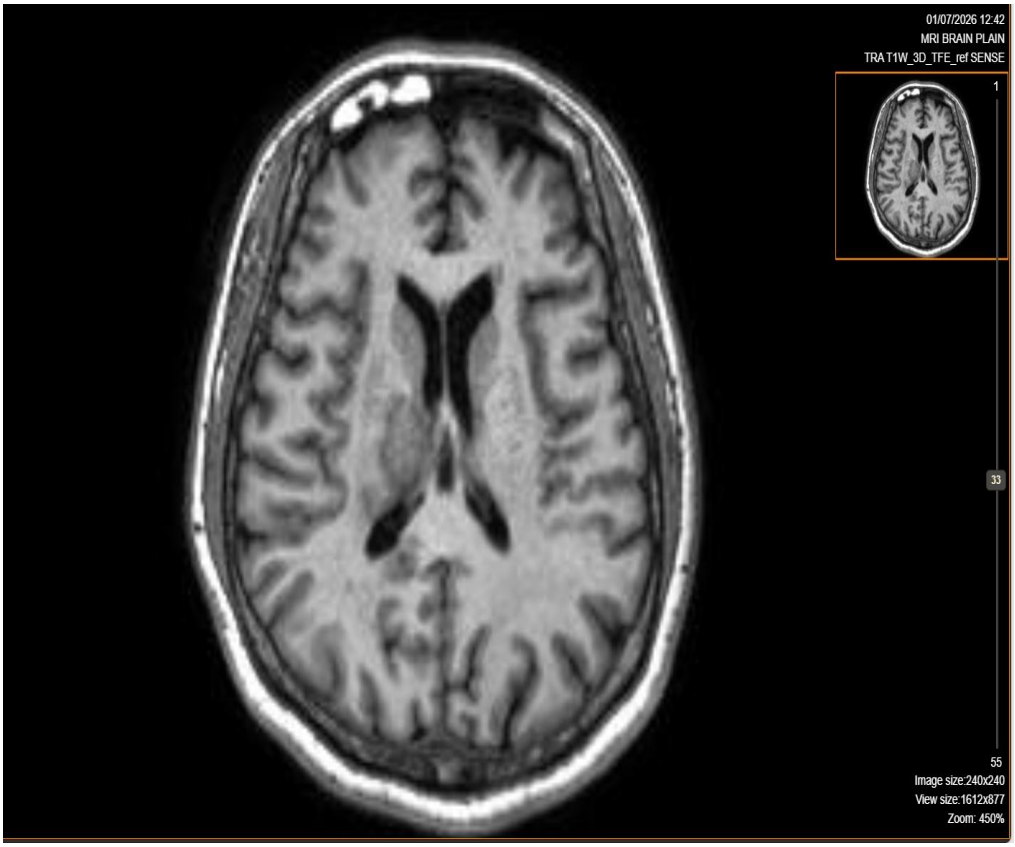
01/07/2026 12:42
MRI BRAIN PLAIN
TRA T1W_3D_TFE_ref SENSE
1
33
55
Image size:240x240
View size:1612x877
Zoom: 450%

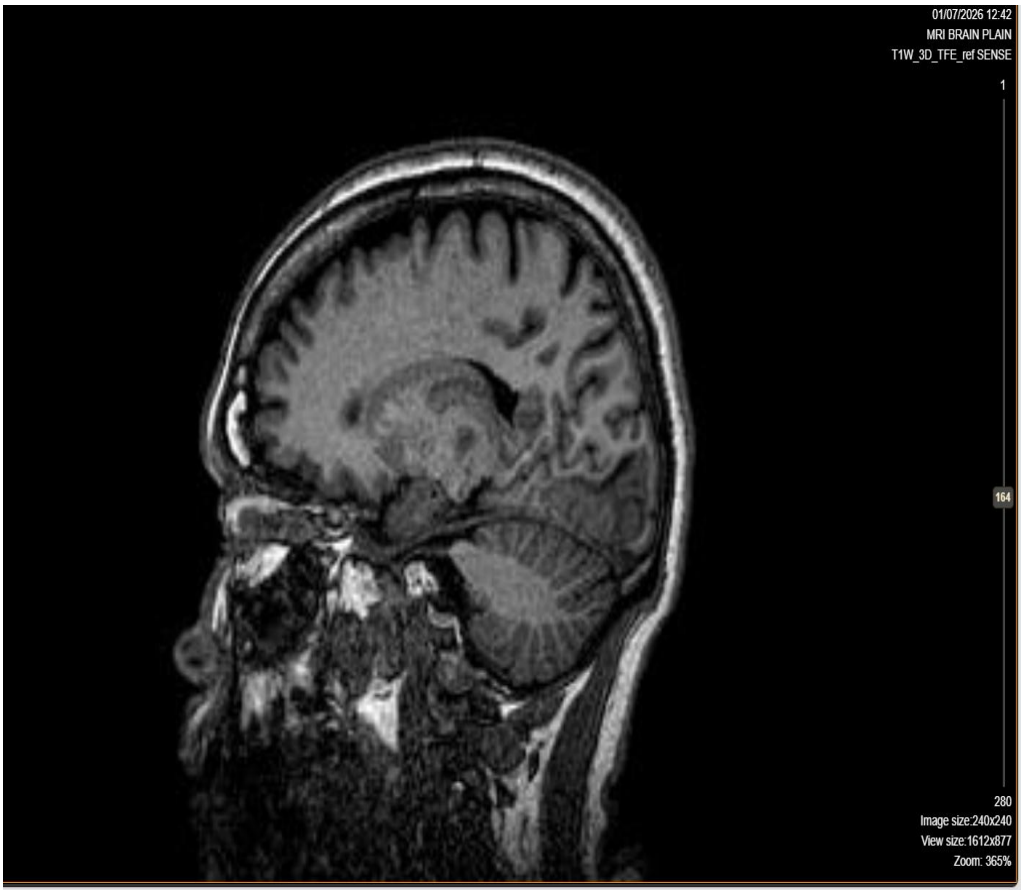
01/07/2026 12:42
MRI BRAIN PLAIN
T1W_3D_TFE_ref SENSE
1
164
280
Image size:240x240
View size:1612x877
Zoom: 365%

Figure 3I. Multiplanar T1-weighted structural imaging.

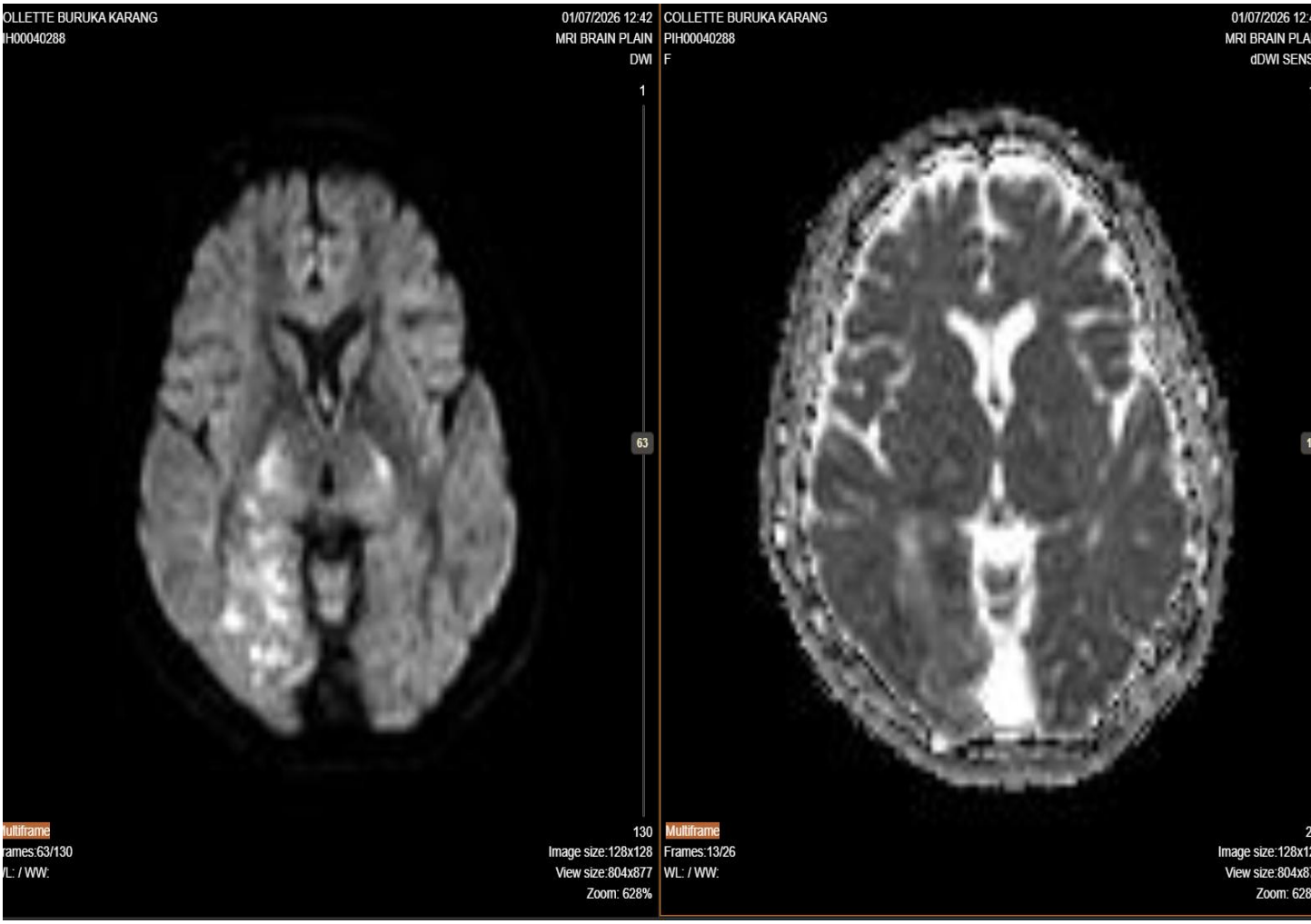

Figure 3J: Integrated DWI and ADC mapping correlation.

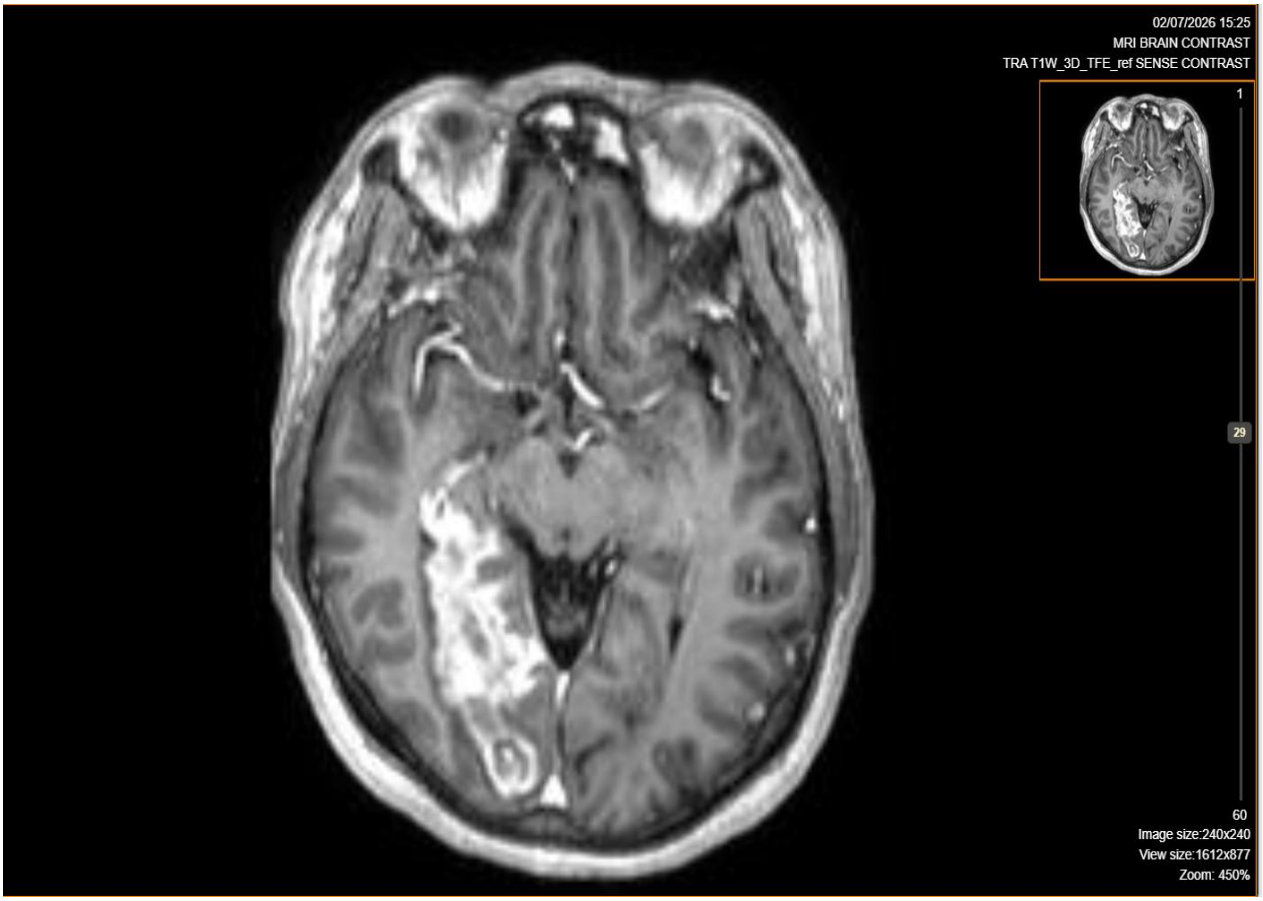
02/07/2026 15:25
MRI BRAIN CONTRAST
TRA T1W_3D_TFE_ref SENSE CONTRAST
1
29
60
Image size:240x240
View size:1612x877
Zoom: 450%

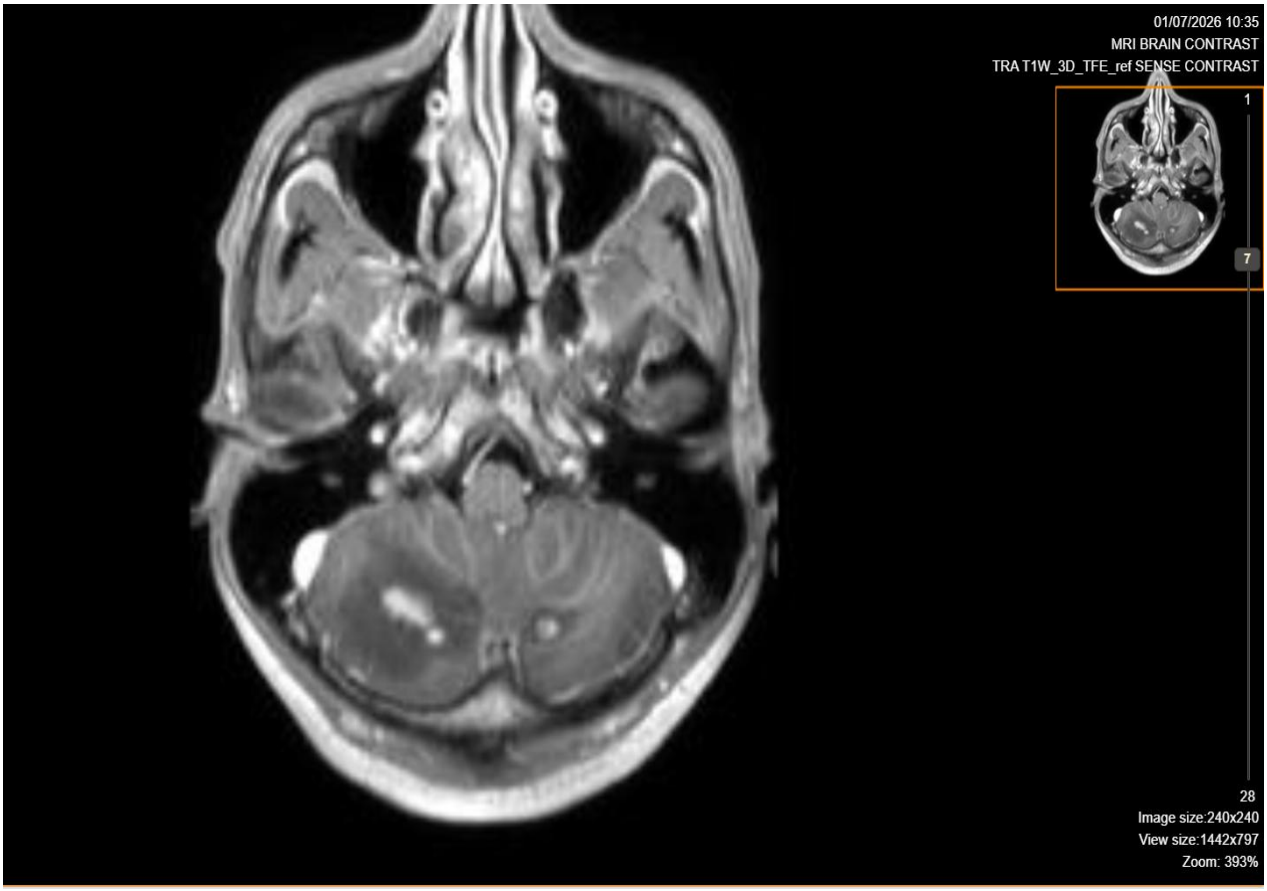
01/07/2026 10:35
MRI BRAIN CONTRAST
TRA T1W_3D_TFE_ref SENSE CONTRAST
1
7
28
Image size:240x240
View size:1442x797
Zoom: 393%

Figure 3K: Post-contrast axial enhancement characteristics.

Figure 3L: Post-contrast sagittal distribution pattern.

01/07/2026 12:42
MRI BRAIN PLAIN
TRA_Brain_VIEW_FLAIR SENSE
1
35
50
Image size:256x256
View size:1612x877
Zoom: 342%

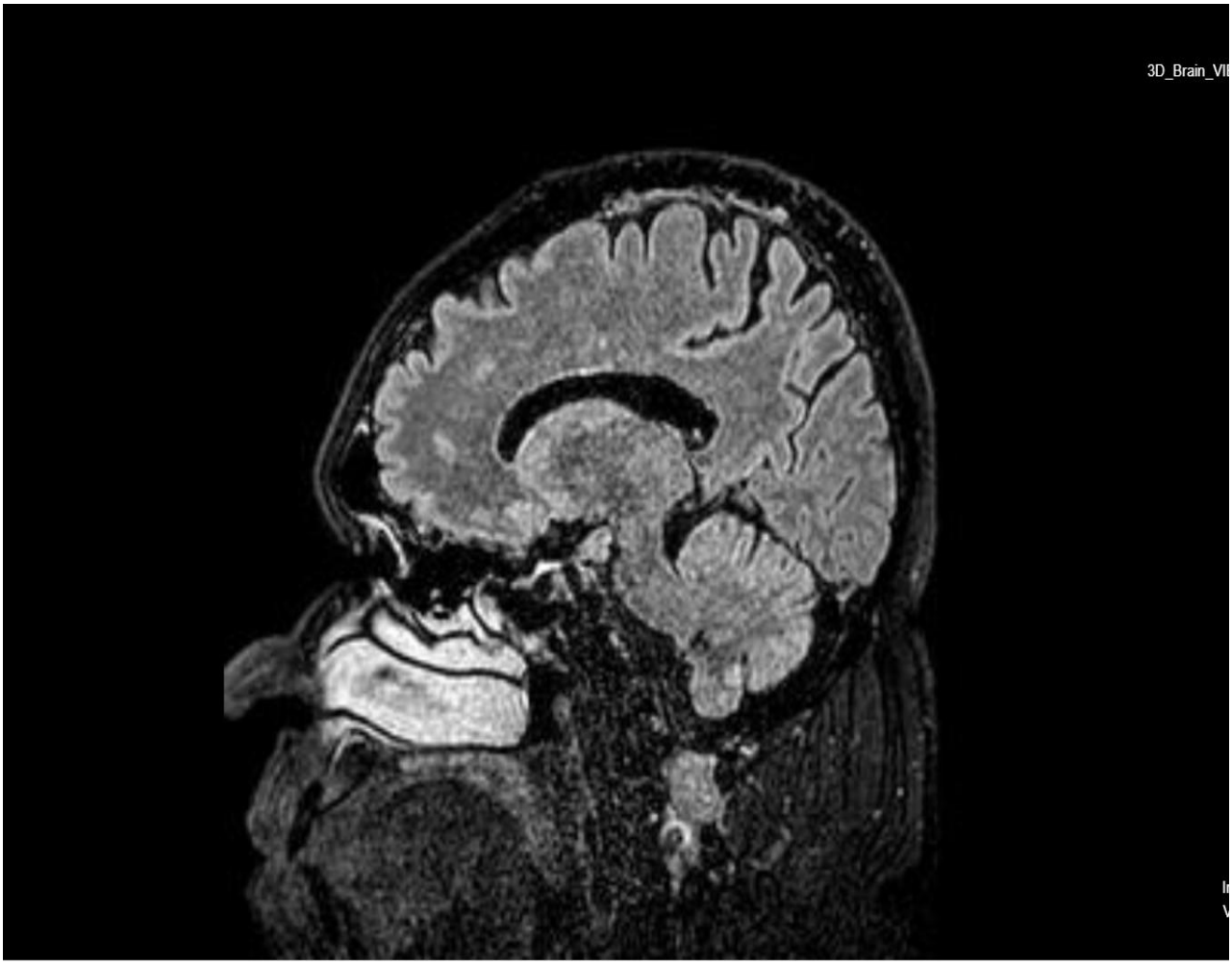
3D_Brain_VI

Figure 3M: Axial and sagittal T2-FLAIR acquisition series.

Case -4 Dumbbell Schwannoma of the Upper Cervical Spine

A 49-year-old patient presented with a more than one-year history of progressive headache, gait disturbance, and difficulty walking, associated with overflow urinary incontinence. Aside from deep white matter T2/FLAIR hyperintensities corresponding to small vessel disease, a subtly enhancing C1–C2 neural foraminal dumbbell-shaped lesion was noted.

Figure 4A. Sagittal T2-weighted image demonstrates a lobulated, heterogeneously hyperintense lesion centered at the C1–C2 neural foramina.

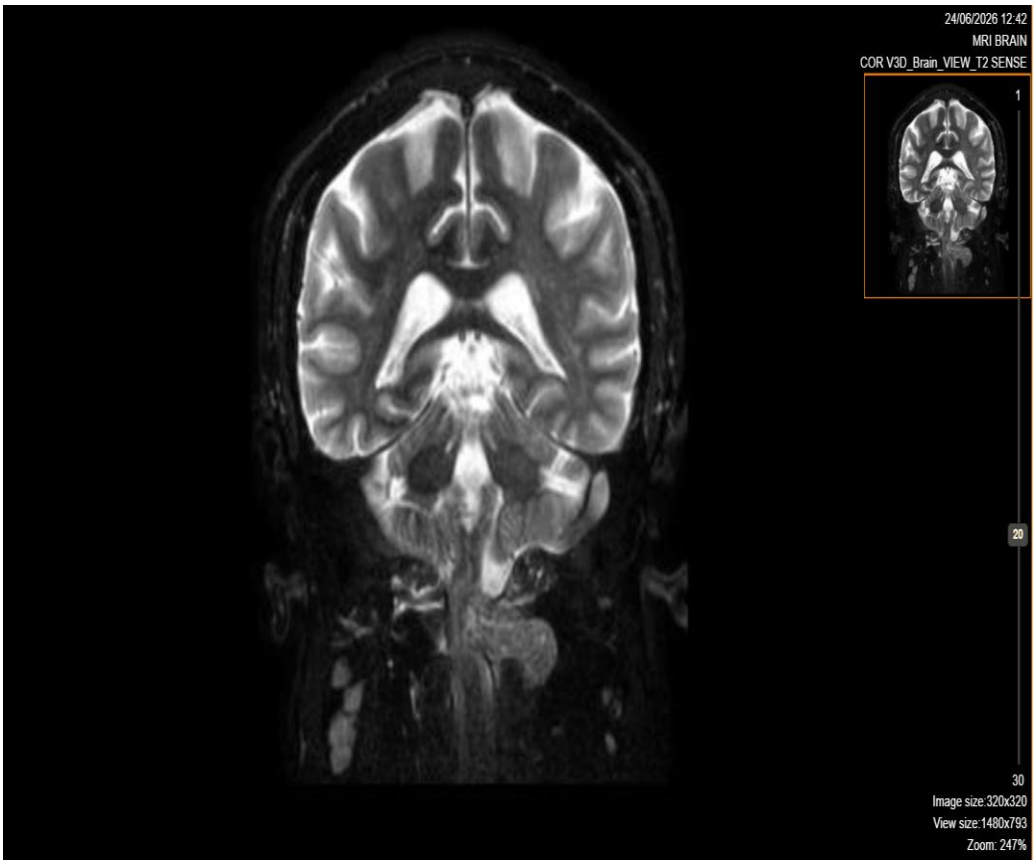

Figure 4B. Coronal T2-weighted image at the C2 level demonstrates the classic "dumbbell" configuration, with a predominantly T2-hyperintense mass extending through and causing scalloping of the neural foramina.

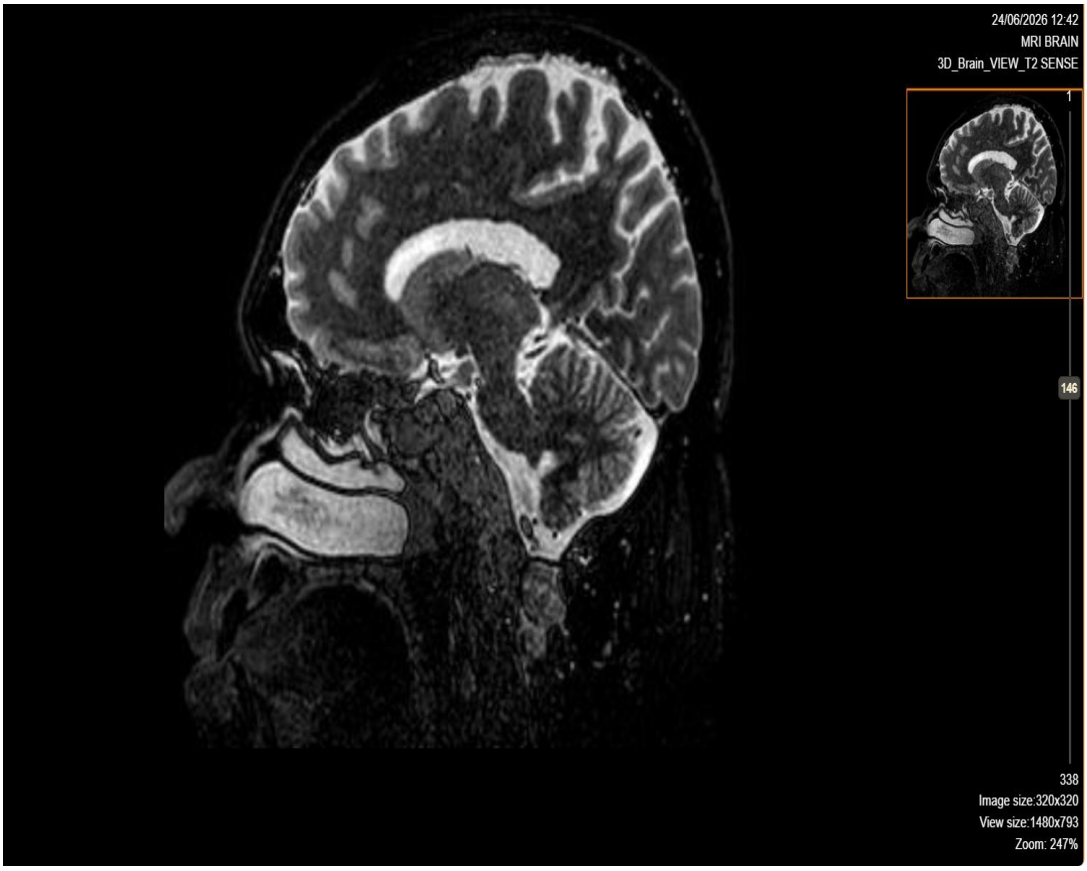

Figure 4C. Sagittal T2-weighted image at the C2 level demonstrates a lesion in the neural foramina with a predominantly T2-hyperintense mass extending through and causing scalloping of the neural foramina.

Figure 4D. Axial T2-weighted image demonstrates the dumbbell sign, with the mass extending through the left C1–C2 foramen into the upper paravertebral region.

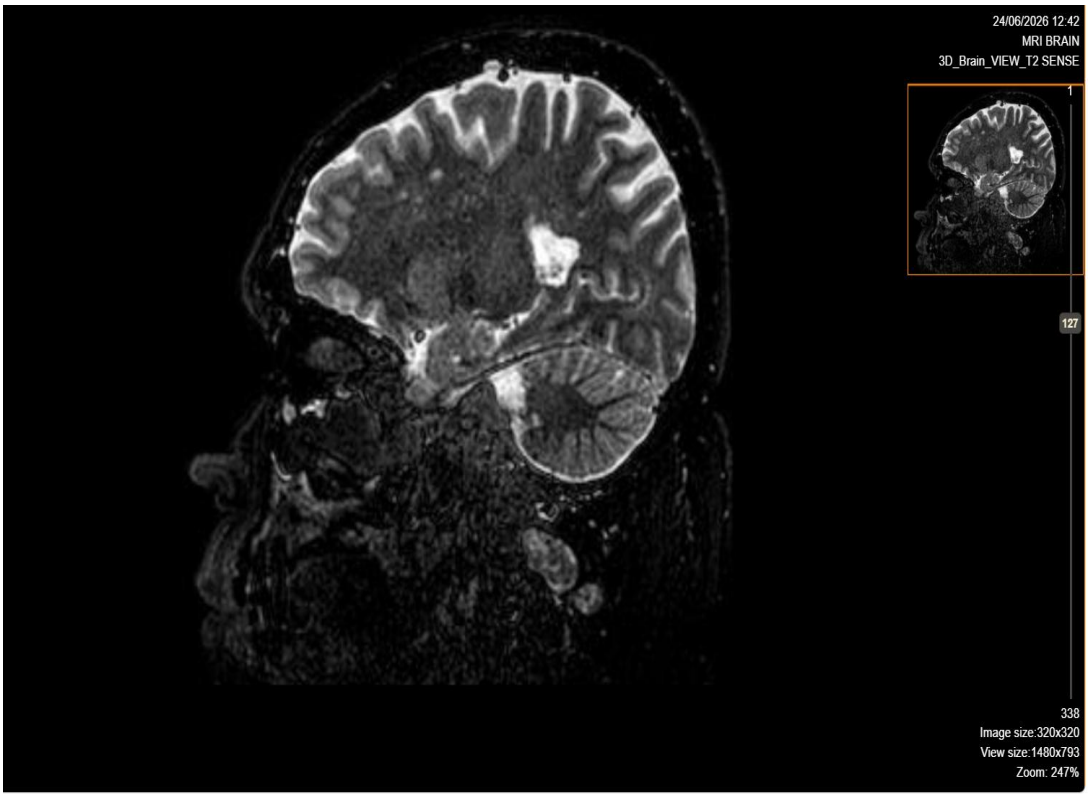

Figure 4E. Two sagittal T2-weighted images at adjacent levels further demonstrate the lesion, confirming its consistent signal characteristics and extent.

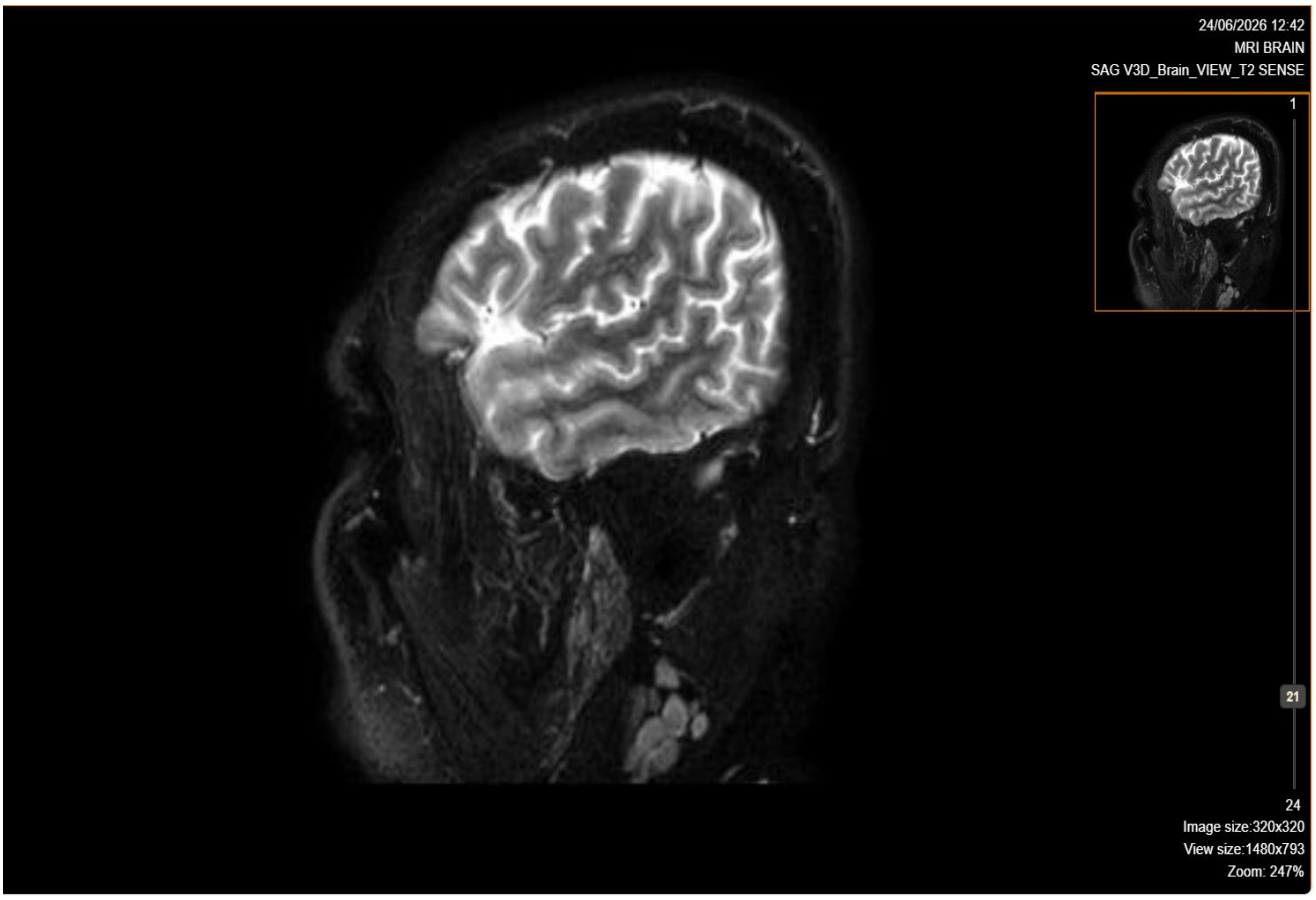

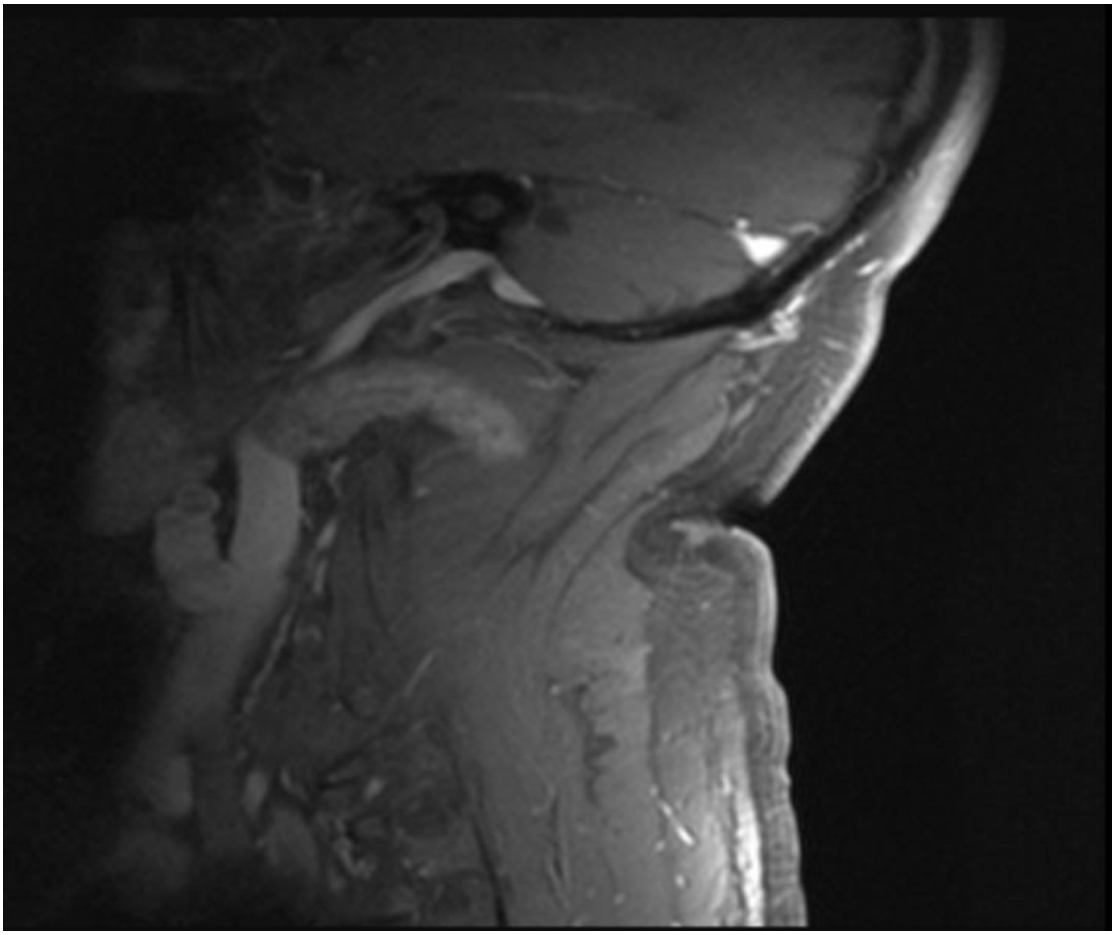

Figure 4F. Contrast-enhanced T1-weighted image demonstrates minimal enhancement of the C1–C2 neural foraminal lesion.